137

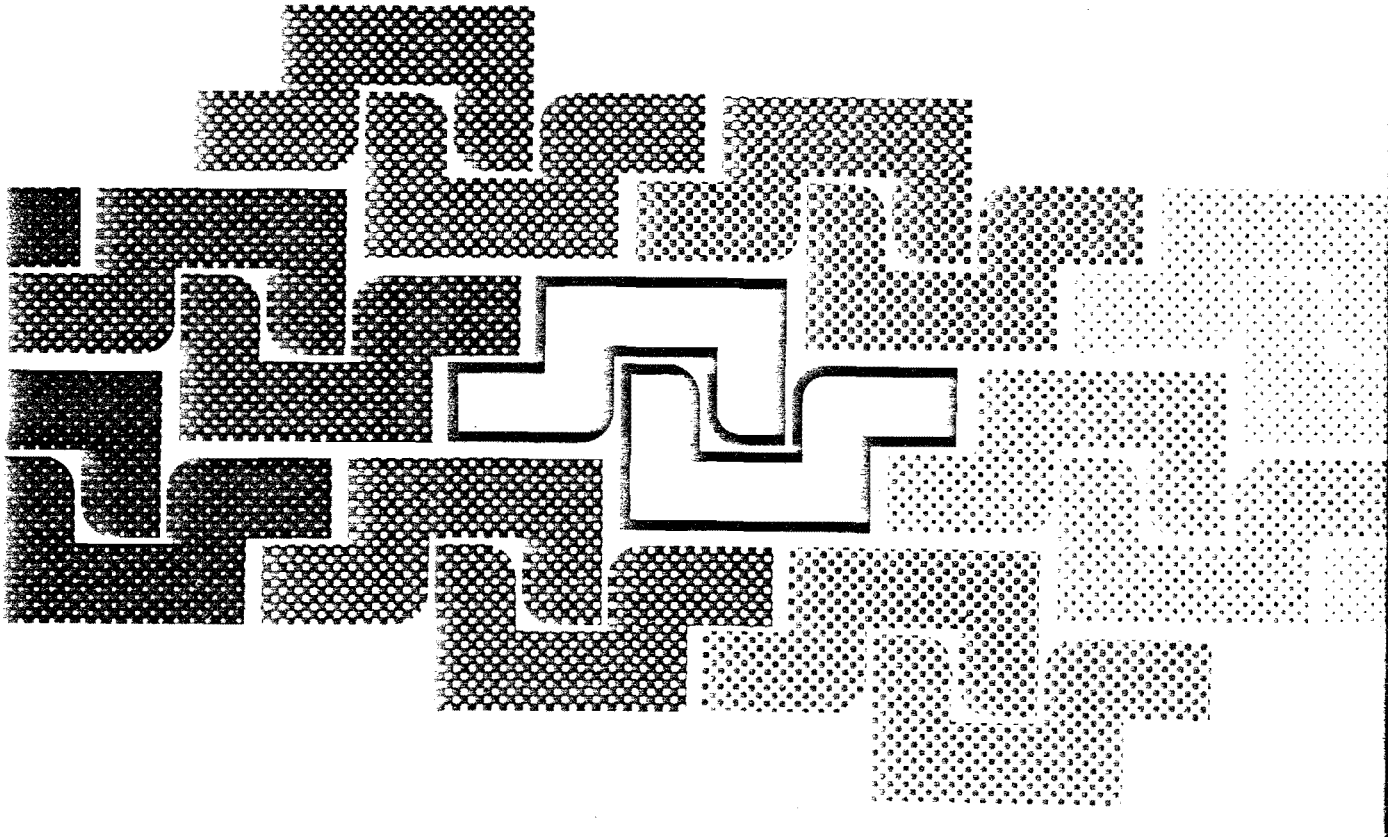

Microscopic Simulations of Complex Flows

Edited by

Michel Mareschal

NATO ASI Series

IRREVERSIBLE PROCESSES FROM REVERSIBLE MECHANICS*

William G. Hoover,[1,2] Carol G. Hoover,[3] Will J. Evans,[2]
Bill Moran,[4] Joanne A. Levatin,[4] and Errol A. Craig[1]

1. Department of Applied Science; University of California at Davis/Livermore
2. Department of Physics; Lawrence Livermore National Laboratory
3. National Magnetic Fusion Energy Computer Center
4. Earth Sciences Department; Lawrence Livermore National Laboratory

[All at Livermore, California, 94550, United States of America.]

ABSTRACT

We describe and illustrate methods for treating many-body irreversible processes using time-reversible deterministic Nosé-Hoover thermostats. In phase space, Lyapunov-unstable multifractal strange attractors are the common feature representing any of these nonequilibrium flows, be they steady, periodic, or transient. This generic behavior is illustrated here for three prototypical one-body problems: steady field-driven diffusive flow in a Galton Board, time-periodic boundary-driven viscous flow of a Lorentz gas, and transient, but time-periodic, compressible flow characterizing a one-dimensional free expansion followed by compression and thermalization.

1. INTRODUCTION

"Real" macroscopic processes are thermodynamically "irreversible". They generate entropy. The microscopic reason underlying this irreversibility is "chaos", or a sensitivity to initial conditions. The discovery and elucidation of chaos is beautifully chronicled in Gleick's book[1] "*Chaos*". Despite its aesthetic appeal, chaos is not always welcome. In his recent California lecture series Yorke[2] termed chaos the "AIDS of Dynamics".

Since the Second World War engineers have used ever-faster computers to simulate the macroscopic continuum mechanics of ever-more-complex flows of gases, liquids, and solids. More recently, particularly in the last five years, atomistic computer experiments have been successfully modeling these same flows, with the motion equations of microscopic atomistic mechanics[3].

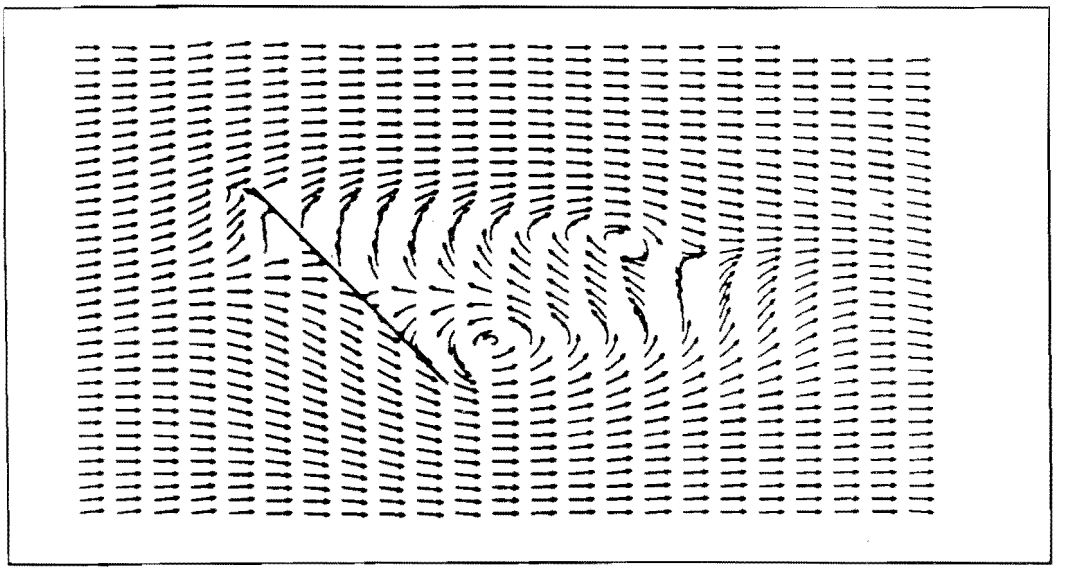

FIGURE 1. Hard-sphere streamlines in a three-dimensional flow past an inclined splitter plate. Each arrow indicates the instantaneous direction of velocity of approximately 50 hard spheres.

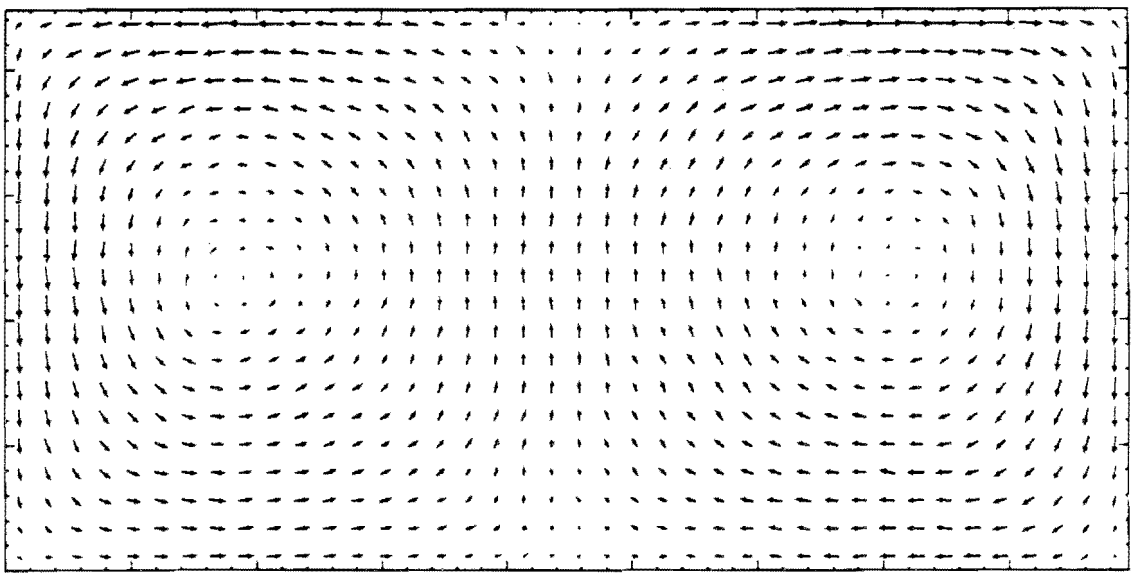

FIGURE 2. Hard-disk velocities for a time-averaged Rayleigh-Bénard flow. The two convective rolls shown are driven by the lower (hot) and upper (cold) boundaries in the presence of a vertical gravitational field.

Meiburg[4] established that microscopic atomistic mechanics can simulate macroscopic hydrodynamic flows. He simulated the flow of a dense viscous fluid of hard spheres past a "splitter plate" by following the motion of 50,000 atoms in three space dimensions. His spatially-averaged streamlines are shown in Figure 1.

A more complicated flow, with stationary hot and cold boundaries, is the heat-conducting Rayleigh-Bénard flow[5] shown in Figure 2. In the Rayleigh-Bénard system, a sufficiently strong gravitational field, combined

with two heat reservoirs, hot at the bottom and cold at the top, can drive a compressible fluid into rotational motion. For sufficiently strong driving, buoyant forces, fed by thermal expansion, generate eddy currents which then dissipate vortical energy through viscosity. In this Rayleigh-Bénard case the fixed-temperature boundary conditions are stationary but the responding currents typically fluctuate in time. More complicated time-dependent problems can involve boundary conditions with either periodic or transient time dependences.

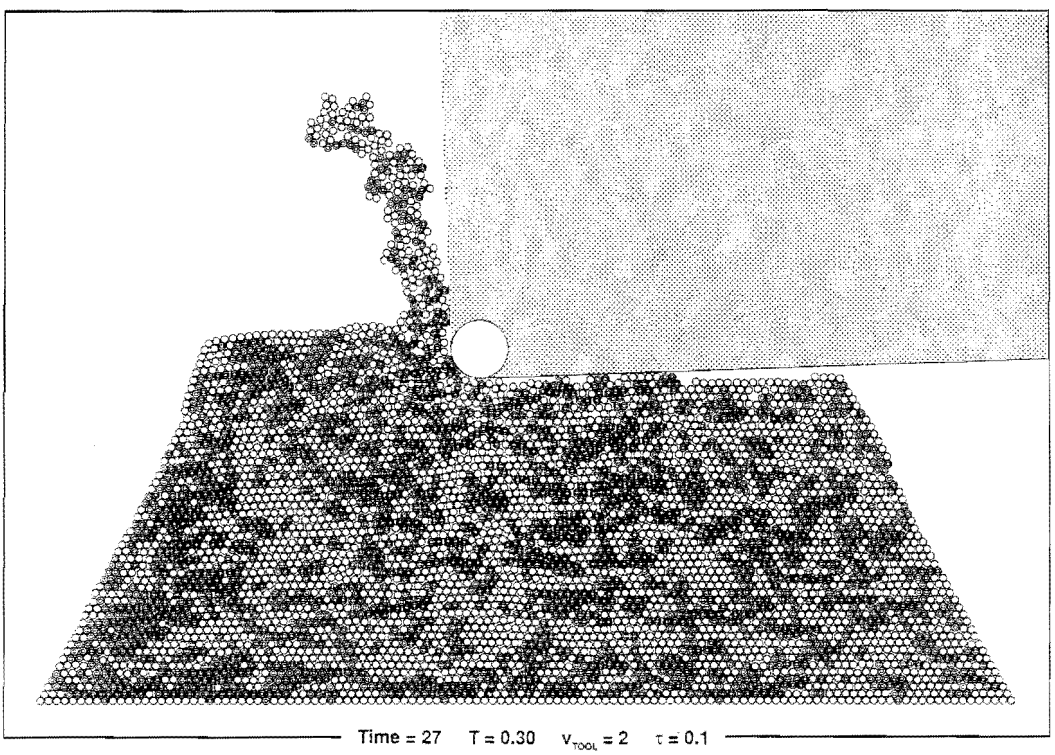

FIGURE 3. Two-dimensional embedded-atom simulation of the diamond turning of a metal workpiece. The "tool", representing a diamond chip with a nanometer radius of curvature, is driven into the crystal at about one-tenth the speed of sound. The crystal is thermostatted at about two-thirds the melting temperature by the two rows of Nosé-Hoover particles adjacent to the base of the crystal. The atoms with higher-than-average potential energy have been shaded.

Both the macroscopic hydrodynamic and the microscopic atomistic approaches have been applied to the convective Rayleigh-Bénard problem. In Lorenz' seminal paper[6] describing the impact of chaos on weather, "Deterministic Nonperiodic Flow", a classic macroscopic caricature of this flow is described. This was the paper that initiated widespread interest in chaotic dynamics.

Even the nonchaotic completely-static small-Rayleigh-number case has some interest as an application for irreversible thermodynamics, the study of processes which generate entropy. In a heat-conducting fluid, even in the absence of gravity, the external entropy loss, at the bottom, $-(dQ/dt)/T_{HOT}$, is less than the external entropy gain, at the top, $+(dQ/dt)/T_{COLD}$. The net result is the entropy increase guaranteed by the Second Law of Thermodynamics.

More complicated solid-state flows, such as the nanometer-scale machining simulation[3] illustrated in Figure 3, involve sources or sinks for plastic or viscoelastic work as well as for heat. Here the microscopic approach is absolutely necessary because the characteristic lengths involved, a few atomic spacings, are too small for the continuum approximations to plastic flow and heat flow to apply.

Meiburg's splitter-plate simulation[4] involved 50,000 particles far from equilibrium. Even earlier the purely-equilibrium Monte Carlo method had been applied at similarly large scales. Beginning with Farid Abraham's announcement[7] of his 161,604-atom computer experiments simulating rare-gas atoms adsorbed on graphite, it became widely appreciated that we can simulate truly macroscopic systems, with sizes corresponding to those studied in laboratory experiments.

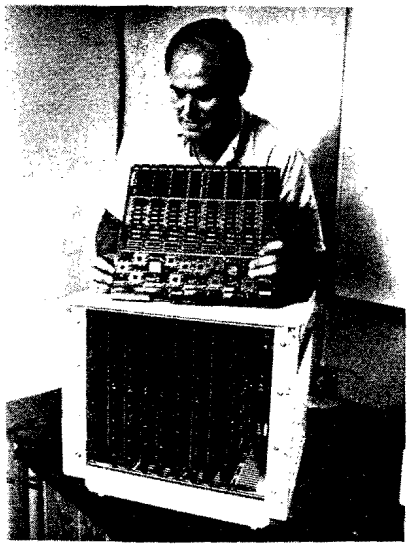

FIGURE 4. DeGroot's SPRINT Multiprocessor. The 64 $500 processors can simulate the cutting process shown in FIGURE 3 at the same clock speed as does a $10,000,000 CRAY computer.

To simulate ever-larger sizes, current research in both microscopic and macroscopic simulations is concentrating on using "multiprocessors". These machines increase computer capabilities about one thousandfold. A recent tabletop model, de Groot and Parker's "SPRINT" machine[8], with 64 parallel processors, is shown in Figure 4. Scaling up such machines should lead soon to a widespread capability for simulating microseconds of real time dynamics for systems with millions of degrees of freedom. Such simulations require hardware outlays of millions of dollars, and programming efforts measured in man-years. Nevertheless, the longterm trend toward parallelism is already clearly established. The major problem with present and projected large-scale calculations is displaying the results in order to "understand" them. This display step is still hard, and time consuming, in three dimensions. Large data files typically require *days* to transport and process.

On the other hand, much of the fundamental physics can be understood by studying much smaller two-dimensional systems for which

detailed averages over *millions* of bins for *billions* of timesteps can be accumulated on current supercomputers. Analogs of many-body macroscopic diffusive, viscous, and heat-conducting dissipative flows can be found on an even much smaller microscopic scale, with just a few degrees of freedom, using the same many-body time-reversible atomistic equations of motion. We return to this idea, with three examples, in Section 5.

We have adopted Boltzmann's interest: relating macroscopic irreversibility to microscopic mechanics. It has only recently been recognized that Second-Law irreversibility can arise naturally even in small systems with two or more degrees of freedom. This recognition was slow in coming because traditional textbook mechanics (Newtonian or Lagrangian or Hamiltonian) predates thermodynamics, and accordingly there was no traditional means for describing *thermo*dynamic properties such as temperature and heat flow. The link between mechanics and thermodynamics is basic and straightforward nevertheless. It can be established by adopting the ideal-gas definition of temperature and the microscopic mechanical definitions of momentum and energy fluxes as the analogs of the macroscopic pressure tensor and heat flux vector.

In an atomistic Boltzmann-Gibbs statistical description the microscopic mechanical state of a classical system includes the complete list of coordinates and momenta for all the degrees of freedom. This information is pictured as specifying a point in many-dimensional "phase space". The equations of motion then generate a "flow" of probability, traditionally written in terms of a time-dependent probability density f(q,p,t) in that space. The probability density f is pictured as representing the "ensemble" flow of many similar discrete systems in space, all obeying the same motion equations, but not interacting with each other. The integral of f, over the whole {q,p} space, is constant, representing the total number of systems in the "ensemble" of systems undergoing investigation.

For conservative Hamiltonian mechanics the generalized (phase-space) flow "velocity" v is composed of both coordinate and momentum contributions, v = (dq/dt,dp/dt), and follows Hamilton's equations of motion:

$$dq/dt = +(\partial H/\partial p) \qquad dp/dt = -(\partial H/\partial q)$$

The divergence of the probability current fv, computed locally as the difference of flux contributions gives the local (fixed q and p) time-rate-of-change of f:

$$(\partial f/\partial t)_{\text{HAMILTON}} = -\nabla\cdot(fv) = -(\partial/\partial q)(fdq/dt) - (\partial/\partial p)(fdp/dt)$$

Then, using the velocity and acceleration equations from Hamilton's equations of motion, we find that $(\partial/\partial q)(dq/dt) = (\partial^2 H/\partial q\partial p)$ and $(\partial/\partial p)(dp/dt) = -(\partial^2 H/\partial p\partial q)$ sum to zero, leading to the usual comoving (or "Lagrangian") form of Liouville's theorem:

$$df/dt = (\partial f/\partial t) + (dq/dt)(\partial f/\partial q) + (dp/dt)(\partial f/\partial p) = 0$$

Conservation of probability, f⊗, where ⊗ is a comoving phase-space hypervolume element, then establishes the relations:

$$d\ln(f\otimes)/dt = d\ln f/dt + d\ln\otimes/dt = d\ln\otimes/dt = 0$$

It is not so well known that all these relations hold even in the case that the forces F are explicit functions of time, as, for instance, in a driven oscillator system.

These deceptively simple Liouville Theorem results, that the comoving probability density f and phase-space hypervolume ⊗ don't change with time, disguise the incredibly complex deformation and rotations generated by nonlinear chaotic dynamics. The basic phase-space deformation mechanism, the Smale horseshoe, is indicated in Figure 5. Successive passes of a comoving hypervolume through those parts of phase space where bending and folding occur produce a multilayered ($2 \rightarrow 4 \rightarrow 8 \rightarrow 16 \rightarrow \ldots$) "fractal" structure with a complexity that increases exponentially fast with time.

Smale's horseshoe deformation is steady. The effects of the process, a repeated bending and folding, steadily penetrate to smaller and smaller scales. The classic space-filling Peano curve, also shown in the same Figure 5, is different. The Peano construction is nonsteady, requiring successivly more-refined deformations, at smaller and smaller scales, as "time" proceeds.

The characteristic time for Smale's exponential bending and folding is the "Lyapunov time". It is of the same order as the collision time and leads to phase-space structures of incredible complexity and beauty for systems with only a few degrees of freedom. In many-body systems the *rotation* of phase-space trajectories occurs on an even faster scale than does the bending and stretching. The resulting geometric complexity lies at present well beyond our descriptive abilities.

The determinism underlying the elegant Liouville description and Smale's phase-space folding would no longer apply if we were to follow the traditional approach to "understanding", or at least simulating, irreversible processes. This well-entrenched recipe proceeds by introducing both friction and "noise" (or "randomness") through Langevin modifications of the motion equations. This approach is obsolete. It suffers from two defects: the stochastic dynamics it generates is neither time-reversible nor deterministic. As a consequence, a Langevin dynamics phase-space flow no longer follows Liouville's Theorem. The twin defects of the Langevin approach complicate analysis and limit reproducibility of results. In this paper we will outline the progress made during the past 15 years in treating irreversible processes with nonequilibrium molecular dynamics. This approach follows Gauss and Lagrange by incorporating (thermal) constraints directly into deterministic and reversible equations of motion. The new equations yield simple analogs of the Liouville Theorem, giving an exact description of the deformation of comoving volume elements in phase space.

The new methods resemble the classical ones in that the fundamental flows in phase space are simple, but the new methods are not Hamiltonian. The starting point is still the same, the phase-space continuity equation satisfied by *any* kind of mechanics with differentiable equations of motion:

$$(\partial f/\partial t)_{\text{ARBITRARY}} = -\nabla\cdot(f\mathbf{v})$$

Here v is again a generalized phase-space velocity, a vector made up of all the time-rates-of-change of the phase-space variables describing the problem. The generalized gradient operator ∇ is similarly a vector sum of phase-space derivatives with respect to these same variables. We illustrate the generalized flow in Figure 6 for a space spanned by coordinates {q}, momenta {p}, and friction coefficients {z]. We will discuss friction coefficients at length in what follows. In any direction in such a space the flow of probability through an area dA during a time interval dt is the product of (i) the probability density f, (ii) the flowvelocity v multiplied by the perpendicular element of area dA, and (iii) the time interval dt. In the example shown in Figure 6, during the time interval dt the flow out of the volume element and parallel to the p direction, through the face $dA = dqd\zeta$ is $f(dp/dt)dAdt$. By summing *pairs* of such contributions, from opposite faces, the continuity equation can be derived. For equilibrium Hamiltonian systems this result is called "Liouville's Theorem".

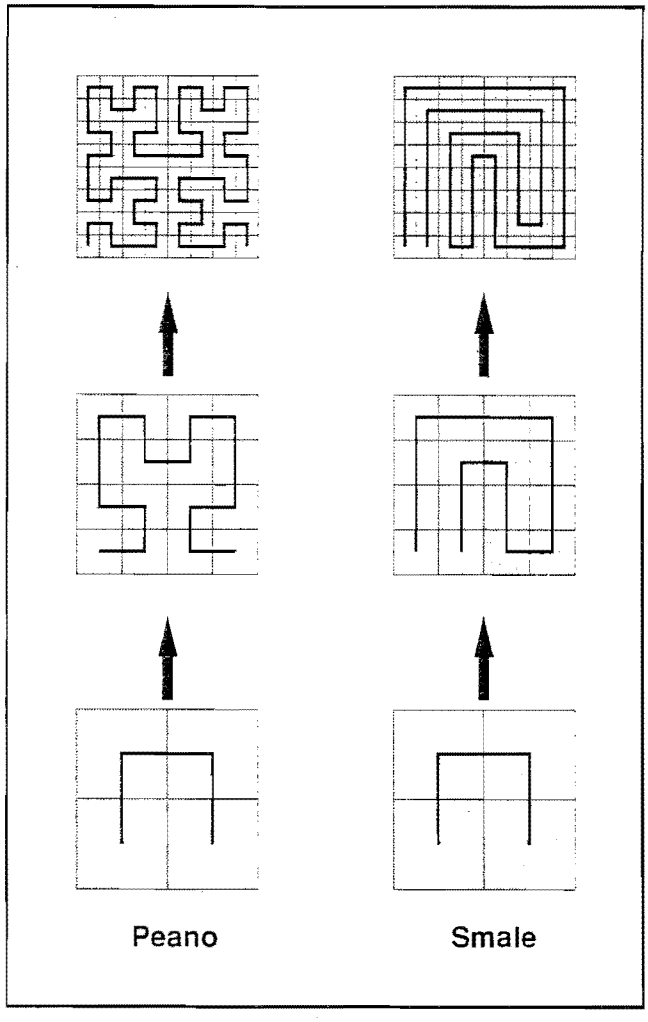

FIGURE 5. The Peano curve and the Smale Horseshoe deformation. Though both constructions have ergodic limits that come arbitrarily close to every point the Peano curve requires successively smaller and smaller scales of deformation while the Smale construction relies on a repeated large-scale bending and stretching. The Smale Horseshoe is a faithful caricature of real phase-space deformation.

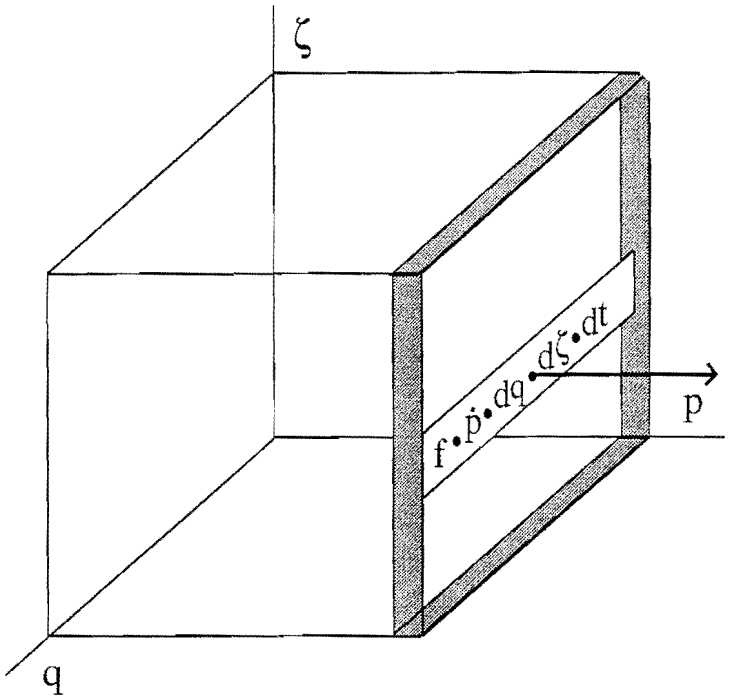

FIGURE 6. The flow from a phase-space hypervolume element is the product of a density f, a perpendicular velocity, dp/dt for the face shown here, a cross-sectional area, here dqdζ, and the time interval dt.

Liouville's Theorem establishes that the motion given by Hamilton's equations, even with time-dependent forces, takes place at *constant* probability density and *constant* hypervolume in a comoving frame. Heat flow gives new results. A *transfer* of heat, ΔQ, from the surroundings into the system, *changes* not only the phase-space probability density, as $e^{-\Delta Q/kT}$, but also the comoving hypervolume, as $e^{+\Delta Q/kT}$, so that df/dt and d⊗/dt are both *nonzero*. Because the time-averaged kinetic energy, $\langle \Sigma p^2/2m \rangle$, is the direct mechanical measure of thermodynamic temperature, thermal constraints are implemented by modifying the time evolution of the momenta. The simplest possible modification of the equations of motion describing heat transfer incorporates frictional forces,

$$F_{\text{FRICTIONAL}} = -\zeta p$$

where ζ is a "friction coefficient". Such forces have proved very useful, both at and away from equilibrium. We describe the corresponding "Nosé-Hoover" version of this development, which began with Nosé's 1984 work, in the next section.

2. NOSE-HOOVER MECHANICS

A "new" approach related to an "old" idea (Gauss' 1829 Principle of Least Constraint) was developed by Shuichi Nosé[9] in his post-doctoral work with Mike Klein, in Canada. Nosé discovered that he could reproduce Gibbs' canonical and isothermal-isobaric distributions, with fluctuating energy and volume, by modifying traditional mechanics.

Let us consider here the simplest of Nosé's modified dynamics, corresponding to Gibbs' equilibrium canonical distribution,

$$f(q,p)_{\text{CANONICAL}} \propto e^{-H(q,p)/kT}$$

Nosé reproduced this distribution by using purely deterministic and time-reversible equations of motion based on a clever modification of Hamiltonian mechanics. It is unfortunate that the approach Nosé pioneered involved a wholly unnecessary "time-scaling" as well as an extraneous distinction between "real" and "virtual" variables. These twin distractions have contributed to misunderstandings of his work's significance[10]. At equilibrium, the end result of Nosé's approach is simply to add a time-varying frictional force to the usual Hamiltonian equations of motion. The result is called the "Nosé-Hoover" equation of motion to indicate the absence of time-scaling and virtual variables:

$$(dp/dt)_{\text{HAMILTON}} = F(q)$$

$$(dp/dt)_{\text{NOSÉ-HOOVER}} = F(q) - \zeta_{NH}p$$

In this form the friction coefficient ζ_{NH} itself obeys a first-order ordinary differential "integral-feedback" equation linking its time-history to the temperature T imposed on the "thermostatted" degrees of freedom:

$$d\zeta_{NH}/dt = [(p^2/mkT) - 1]/\tau^2.$$

If *several* degrees of freedom are to be constrained in this way, with a common friction coefficient, then the righthand side is to be averaged over *all* these degrees of freedom. The thermostat relaxation time t is "phenomenological" (that is, a free parameter). We follow Maxwell, Boltzmann, and Gibbs in identifying the ideal-gas temperature scale, $\langle p^2/mk \rangle \equiv T$, as the fundamental (mechanical) definition of temperature. In any stationary or time-periodic process $\langle d\zeta/dt \rangle$ vanishes and the "definition" of temperature just described is also a dynamical identity.

For ergodic systems, the motion equations just given generate the canonical distribution in phase space. The equations are novel. They include both macroscopic and microscopic variables side by side. But just as in traditional microscopic mechanics, the Nosé-Hoover equations are time-reversible, with both z and p changing sign along with time on a reversed trajectory. Straightforward generalizations of them generate the isothermal-isobaric phase-space distribution. The thermostat forces $\{-\zeta p\}$ operate by taking up or giving off heat according to the past history of the instantaneous ideal-gas temperature, $T(t) \equiv p^2/mk$. If p^2/mk exceeds the desired temperature T for a particular degree of freedom the friction increases. If p^2/mk is less than T then the friction tends to decrease, and, for negative values, *adds* energy to the system. This time-varying friction makes additional random or stochastic forces of the Langevin type unnecessary.

Brad Holian suggested a constructive derivation of these "Nosé-Hoover" non-Hamiltonian equations of motion which is much simpler than Nosé's Hamiltonian approach. Begin by *assuming* a friction-coefficient

equation of motion with a friction coefficient $\zeta(q,p)$ depending only on q and p. Then observe that the *only* motion equation for $d\zeta/dt$ consistent with the canonical distribution is Nosé's:

$$d\zeta/dt \equiv [(p^2/mkT) - 1]/\tau^2$$

As a fringe benefit, the equilibrium distribution for ζ (that is, the distribution in an isolated system) turns out to be a simple Gaussian, centered on zero, with the fluctuating frictional effects vanishing [typically as $N^{-1/2}$ or N^{-1} for N degrees of freedom] in the large-system [large N] "thermodynamic limit".

It is interesting that exactly the *same* friction-coefficient form of the equations of motion follows also from Gauss' Principle of Least Constraint, if that Principle is used to impose a constraint force keeping the *kinetic energy* constant.

$$(dp/dt)_{GAUSS} = F(q) - \zeta_{GAUSS}p$$

The recipe for Gauss' friction coefficient looks *different* from Nosé's:

$$\zeta_{GAUSS} = -(d\Phi/dt)/2K$$

where $\Phi(q)$ and $K(p)$ are the potential and kinetic energies. But, in the limit that Nosé's relaxation time t vanishes the coordinate-space trajectories following the Nosé-Hoover equations given above reduce to those generated using Gauss' equations of motion.

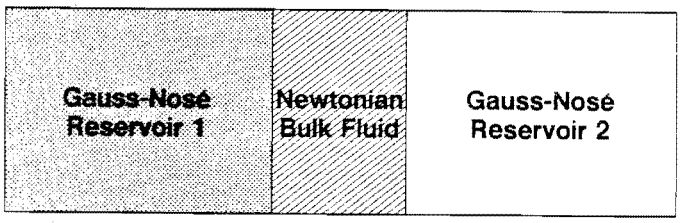

FIGURE 7. Schematic construction of a nonequilibrium steady state. The two boundary regions, stabilized by Gaussian or Nosé-Hoover reservoirs, drive the Newtonian particles sandwiched between them.

More than 30 years after Fermi's pioneering work at Los Alamos, atomistic equilibrium calculations are a well-established and routine undertaking but nonequilibrium techniques are still being developed. And Nosé's ideas, a natural extension of Gauss' "Principle of Least Constraint", are a fertile source of new methods. To study a simple two-temperature heat flow, with hot and cold boundaries, the sandwich construction shown in Figure 7 can be used. In that Figure Newtonian bulk fluid is shown interacting with two "Gauss-Nosé" reservoir regions. Suppose that the lefthand region is hot and the righthand region cold. In the lefthand "hot" region *some* degrees of freedom satisfy thermostatted Nosé-Hoover equations with a "hot" friction coefficient ζ_{HOT}:

$$(dp/dt)_{\text{NOSÉ-HOOVER}} = F(q) - \zeta_{HOT}p$$

$$d\zeta_{HOT}/dt = [(p^2/mkT_{HOT}) - 1]/\tau_{HOT}^2$$

In the righthand "cold" boundary region at least some degrees of freedom satisfy similar thermostatted equations of motion incorporating a "cold" friction coefficient ζ_{COLD}:

$$(dp/dt)_{\text{NOSÉ-HOOVER}} = F(q) - \zeta_{COLD}p$$

$$d\zeta_{COLD}/dt = [(p^2/mkT_{COLD}) - 1]/\tau_{COLD}^2$$

Though this may appear to be nothing more than an "*ad hoc*" way of imposing hot and cold temperatures on selected degrees of freedom, this approach has two real advantages over the old Langevin approach:

First, Nosé-Hoover mechanics makes it possible to predict the *direction* of energy flow consistent with the Second Law of Thermodynamics[11].

Second, the new mechanics also establishes a *quantitative* connection between the macroscopic entropy increase and the mechanical Lyapunov spectrum of the underlying microscopic mechanics[12].

We can establish both results by considering a Nosé-Hoover phase-space flow. Such a flow can have *many* friction coefficients, $\{\zeta\}$, with each coupled to its own particular set of degrees of freedom. The instantaneous values of the friction coefficients fluctuate, but the sum of the time averages, $<\Sigma\zeta>$, is constrained geometrically. It is easy to see, for any bounded region of phase space away from equilibrium (implying nonvanishing heat transfer, $<\Sigma\zeta> \neq 0$), that the *analog* of Liouville's Theorem,

$$df/dt = -f(\partial/\partial p)(dp/dt) = f\Sigma\zeta$$

makes sense *only* if the friction coefficient sum is positive. If instead df/dt were negative, the steady-state f would have to decay to zero and the occupied phase-space volume $\otimes$ would then necessarily diverge. Thus df/dt and $<\Sigma\zeta>$ must both be postive. Accordingly, away from equilibrium the phase volume $\otimes$ must go to zero. This vanishing of the phase volume leads to strange-attractor phase-space structure of the type we illustrate in Section 5.

Nosé's equations of motions have another interesting consequence. They imply directly that the friction coefficients are not correlated with their corresponding temperatures. To see this, multiply the equation of motion for $d\zeta_{NH}/dt$ by $\tau^2\zeta_{NH}$ and time average:

$$\tau^2<\zeta_{NH}d\zeta_{NH}/dt> \equiv <\zeta_{NH}[(p^2/mkT) - 1]> = 0$$

Because ζ_{NH}^2 is bounded, the time average vanishes, leading to the conclusion:

$$<\zeta_{NH}[(p^2/mkT)> = <\zeta_{NH}>$$

This lack of correlation between the instantaneous temperature $p^2/(mk)$ and the friction coefficient ζ_{NH} gives a simple relation between the external surroundings entropy rate-of-change associated with a reversible heat transfer, $(1/T)(dQ/dt)$, and the friction coefficient ζ_{NH}:

$$-(1/T)\langle dQ/dt\rangle = (1/T)\langle \zeta_{NH} p^2/m\rangle = \langle \zeta_{NH}\rangle (1/T)\langle p^2/m\rangle = k\langle \zeta_{NH}\rangle$$

Here, positive ΔQ (or negative friction) corresponds to flow into the system, through the frictional forces, from the "surroundings". Because the requirement that the phase-space volume be bounded implies that $\langle \zeta_{NH}\rangle$ is positive we conclude that the summed heat inputs, divided by the corresponding temperatures, must be negative. In the steady state this means that the corresponding sum for the external heat reservoirs, which extract the heat ΔQ stabilizing the motion, must be positive:

$$dS_{TOTAL}/dt = -\Sigma(dQ/dt)/T > 0$$

Thus Nosé-Hoover mechanics establishes that *the flow of heat must be in the direction consistent with the Second Law*, so that

Work can *only* be converted into Heat

not the other way around. This link between Nosé-Hoover mechanics and the Second Law of Thermodynamics is outlined in Figure 8. In the upper half of that Figure the conservation of probability $f\otimes$, where $\otimes$ is a phase-space volume element, is indicated. Nosé's equations of motion link the change in probability density with time to the friction coefficients $\{\zeta\}$ and simple geometry links the change in volume with time to the Lyapunov exponents $\{\lambda\}$. We discuss these links between the microscopic Lyapunov spectrum, phase-space volume, and fractal strange attractors in the next two sections.

In the bottom section of Figure 8 it is indicated that finite phase-space volume implies that the friction coefficient sum, $\Sigma\zeta$, must be positive, and that this in turn establishes that the production of entropy is positive, the Second Law of Thermodynamics.

Application of Nosé's ideas to irreversible macroscopic problems is straightforward. In a companion paper we describe simulations of high-speed machining operations in which reversible Nosé-Hoover thermostats are used to control the macroscopic temperature of the workpiece. In the present paper we instead develop analogs for macroscopic systems which are chosen for simplicity, to illustrate the qualitative features and logical connections without the complexity of high-dimensionality state-of-the-art molecular dynamics simulations.

The traditional textbook way to study nonequilibrium states is to imagine that they arose as equilibrium fluctuations. For states more than a little different from equilibrium states this is an odd idea. It is conceptually much simpler to focus on driven systems--systems forced away from equilibrium into nonequilibrium steady states. In steady-state nonequilibrium processes chemical potential, velocity, or temperature differences are maintained in the face of diffusive, viscous, and thermal

dissipation.Shock or detonation waves combine *all* of these processes. Figure 9 shows the simple prototypical nonequilibrium system illustrating these steady-states. Black and white are used in the Figure to represent differences in species, velocity, or energy, with the lefthand reservoir a source of black particles and the righthand reservoir a source of white ones. Mixing, described by Fick's Laws of diffusion, Newtonian viscosity, or Fourier's heat conduction, occurs in the middle Newtonian region. Mass, momentum, and energy flow steadily through the system. As a consequence of the nonequilibrium flow heat is continuously generated and flows out of the system into the boundary regions.

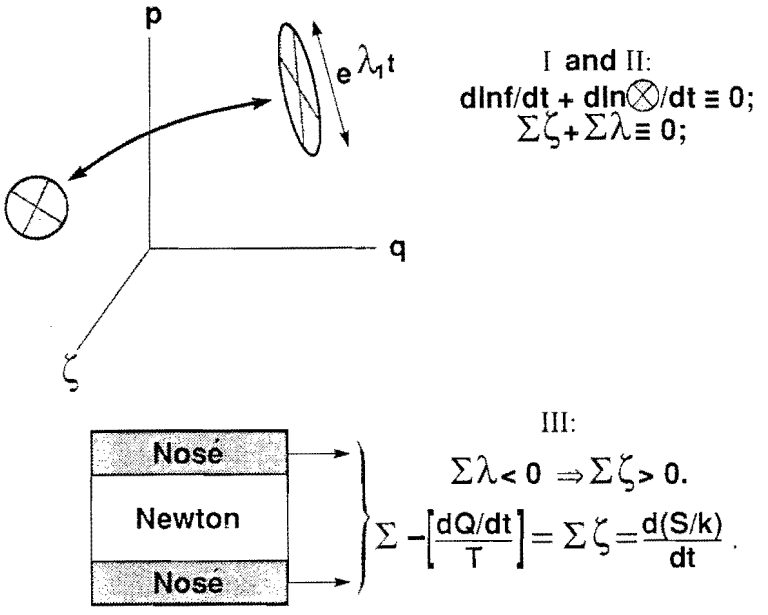

FIGURE 8. Summary of the mechanical basis of the Second Law of Thermodynamics. The upper part of the FIGURE relates probability conservation to the friction coefficients {ζ} and the Lyapunov spectrum {λ}. The lower part indicates the connection of sums of these numbers to the thermodynamic entropy production dS_{TOTAL}/dt.

If we use Nosé mechanics to simulate such a flow we find that the phase-space distribution function f(q,p,t) rapidly collapses, with the ratio f(t)/f(0) diverging as $e^{-\Delta Q/kT}$, with ΔQ negative, onto a zero-volume (decreasing as $e^{+\Delta Q/kT}$) object called a STRANGE ATTRACTOR. Why is the attractor "strange"? First, within the attractor, trajectories separate rapidly from one another, exponentially fast, despite the attractor's having zero volume. Second, there is no probability density on the attractor. The probability per unit volume approaches no limit for smaller and smaller phase-space binnings. The distribution contains irregularities on all spatial scales. This topological behavior is completely unlike the smooth functions to which ordinary calculus applies. Our present understanding of strange-set topology is today still primitive and crude. The existence of these strange phase-space objects depends upon the "Lyapunov instability" of the equations of motion, that is, the tendency for nearby phase-space trajectories to separate from each other exponentially fast, in time.

The shrinking of the occupied phase space and the corresponding collapse and divergence of f(q,p,t) gives rise to a qualitative change in phase-

space topology, a loss of phase-space dimensionality. This loss is macroscopic and depends on the departure from equilibrium. For instance, a cubic centimeter of water, sheared slowly at 1 hertz, has a distribution function f which increases e-fold on a picosecond timescale. The loss of phase-space dimensionality for this case is negligible, of order 1 part in 10^{24}. The much stronger gradients in shockwaves can make the Lyapunov-unstable divergence 24 orders of magnitude faster and the corresponding dimensionality loss 24 orders of magnitude greater. In the next section we discuss the detailed characterization of Lyapunov instability and its consequences.

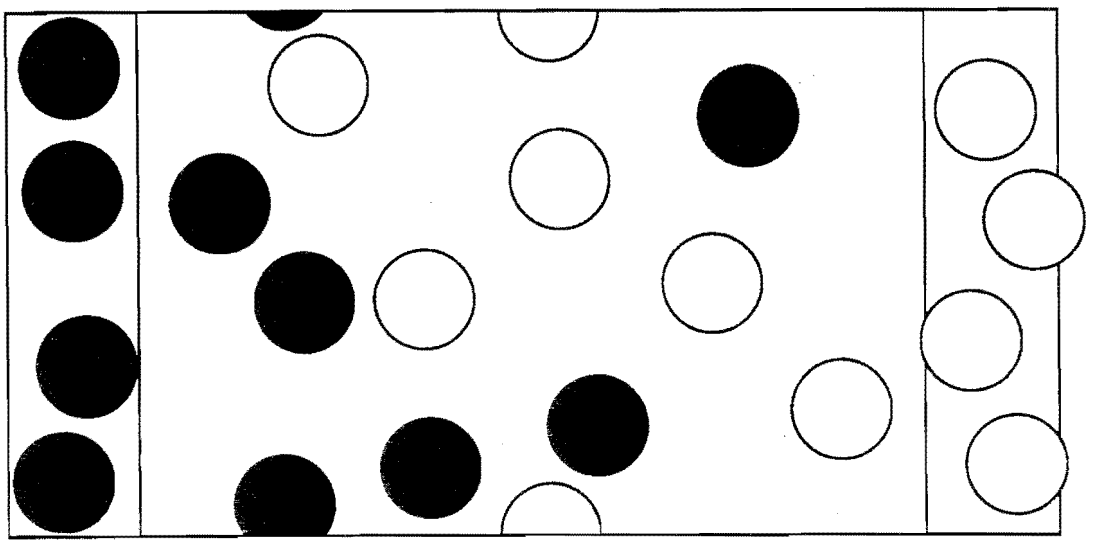

FIGURE 9. A prototypical nonequilibrium problem in which two reservoirs, with characteristic values of the concentration, velocity, or temperature, cause a nonequilibrium mass, momentum, or energy flux through the central Newtonian region.

3. LYAPUNOV INSTABILITY

We have seen that the geometric requirement that stationary states be bounded in phase space breaks the symmetry of the equations of motion, forcing the time development to seek out the direction of phase-space shrinking. In these stationary nonequilibrium continuously-shrinking flows the comoving phase-space hypervolume $\otimes$ exhibits two paradoxical combinations of contraction and expansion properties:

First, the behavior of nearby points in phase space suggests *expansion* rather than contraction, by separating, exponentially fast in time, as the motion goes on. For a simple bouncing-ball illustration[13] of this exponential separation see Figure 10. With each bounce the horizontal offset from the ball's center increases as a geometric series. The resulting exponential instability is best visulized on the semilogarithmic plot shown in the righthand side of the Figure. But, as we have seen, simultaneously with the separating, the comoving *occupied* volume in phase space, $\otimes$, necessarily shrinks, exponentially fast, to zero.

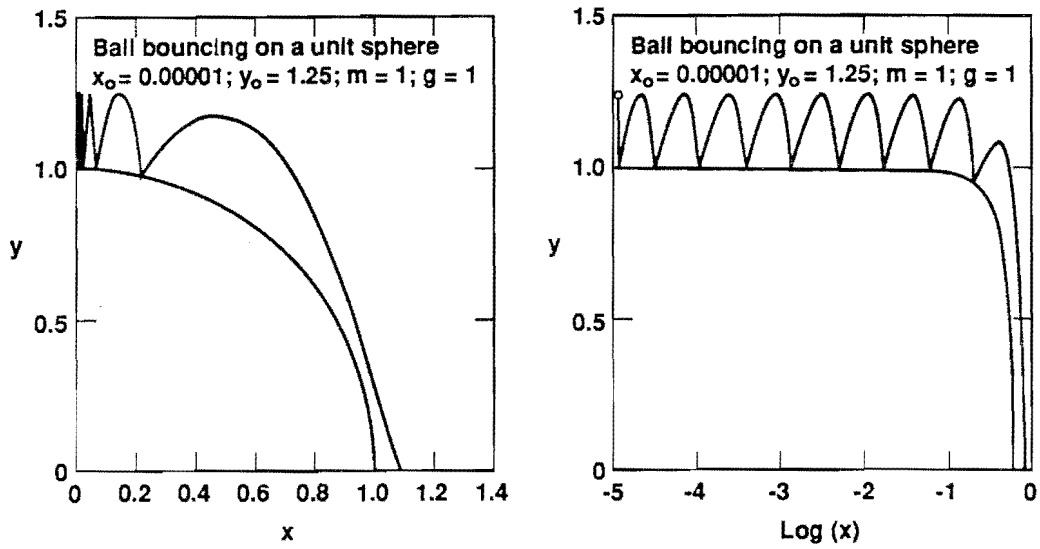

FIGURE 10. A gravity-driven bouncing ball. The Lyapunov-unstable motion causes the horizontal offset from the unstable central fixed point above the ball to increase with each bounce. The exponential character of this instability is illustrated by the logarithmic-scale motion shown on the righthand side of the FIGURE.

Second, at least for the "simple" examples considered here, it appears that the limiting and well-behaved "attractor" set toward which this shrinking motion converges is everywhere arbitrarily close to pathologically unphysical time-reversed "repellor" points which violate the Second Law of Thermodynamics[14].

The first property, expansion and separation, is typical of all strange attractors but the second Second-Law property is not. Most of the maps and flows studied in nonlinear dynamics lack the time reversibility of mechanics. Newtonian and Nosé-Hoover mechanics both exhibit the paradox that to every trajectory obeying the Second Law there is a reversed trajectory which violates it. With this second paradox the zero-volume attractors of nonequilibrium mechanics richly deserve both the appellation "strange" and the study required to make them less so. In this section we first describe the measurement of Lyapunov spectra characterizing attractors. We then review recent results and discuss the link between Lyapunov spectra and static attractor structure. At present the structural analysis of attractors is crude. It is mostly restricted to time-averaged scalar properties of three-dimensional objects and still lacks a classification scheme with which to distinguish attractors from one another.

Among the relatively-crude (because it is time-averaged) ways to analyze the paradoxical strange-attractor motion is the Lyapunov spectrum. To define it we consider the comoving deformation of an infinitesimal phase-space hypersphere, centered on a "reference trajectory" and spanned by the corotating set of infinitesimal orthonormal basis vectors $\{\delta\} = \{(\delta q, \delta p)\}$. In Figure 11 we indicate the rotation of the comoving vectors, shown as arrows, by shading half the hypersphere in which they are embedded. A trajectory segment composed of five equal time steps is shown in Figure 11. Because the comoving and corotating embedding hypersphere is infinitesimal, within it the equations of motion can be linearized relative to those applying at the hypersphere center. This linearization completely avoids the complex

bending and folding associated with the Smale horseshoes of the type shown in Figure 5.

The linearization idea can be applied equally well to equilibrium or nonequilibrium systems. For simplicity, consider the linearized equations appropriate to Hamilton's motion equations:

$$d\delta q/dt = \delta p/m;\ d\delta p/dt = \delta q(dF(q)/dq)$$

or, to simplify and generalize the notation by introducing the dynamical matrix D:

$$d\delta/dt = D\cdot\ \delta$$

These basis-vector equations of motion, just like those of the reference trajectory, are time-reversible, with the signs of δp and dt changing in a time-reversed trajectory. Such a linearized motion would convert a hypersphere to a rotating hyperellipsoid characterized by the exponential growth and decay rates of its (orthogonal) principal axes. These rates, when time-averaged and ordered from the largest, λ_1, to the smallest, λ_N, in an N-dimensional phase space, constitute the "Lyapunov Spectrum" $\{\lambda_i\}$.

An alternative description of this same growth-rate spectrum can be based on the time-averaged deformation of infinitesimal 1-, 2-, 3-, ... dimensional phase-space objects. To generalize the simple property of exponential divergence of the one-dimensional distance between neighboring trajectories, it is natural next to consider the divergence (or convergence) of infinitesimal two-dimensional phase-space areas, followed by three-dimensional volumes, four-dimensional hypervolumes, and so on. When time-averaged, the successive orthogonal growth rates required are again the Lyapunov exponents. The largest, λ_1, describes the rate of divergence of an infinitesimal one-dimensional *length* δr linking two trajectories:

$$\lambda_1 = d\ln\delta r/dt$$

By adding λ_1 to the next largest exponent, λ_2, we get the sum, $\lambda_1 + \lambda_2$, describing the growth rate for a two-dimensional *area* dA defined by three neighboring trajectories:

$$\lambda_1 + \lambda_2 = d\ln\delta A/dt$$

By adding more dimensions we finally reach the last such relation:

$$\Sigma\lambda_i = d\ln\delta\otimes/dt$$

where the sum includes all N Lyapunov exponents and $\delta\otimes$ is a comoving infinitesimal hypervolume element with the full phase-space dimensionality.

Numerical characterization of the complete spectrum of Lyapunov exponents[12] is computationally intensive. What can be done is severely limited by computational speed. In 1989 it is feasible to compute accurate values of hundreds, but not yet thousands, of Lyapunov exponents, and

bending and folding associated with the Smale horseshoes of the type sho in Figure 5.

The linearization idea can be applied equally well to equilibrium nonequilibrium systems. For simplicity, consider the linearized equatic appropriate to Hamilton's motion equations:

$$d\delta q/dt = \delta p/m;\ d\delta p/dt = \delta q(dF(q)/dq)$$

or, to simplify and generalize the notation by introducing the dynamic matrix D:

$$d\delta/dt = D\cdot\ \delta$$

These basis-vector equations of motion, just like those of the referen trajectory, are time-reversible, with the signs of δp and dt changing in a tim reversed trajectory. Such a linearized motion would convert a hypersphere a rotating hyperellipsoid characterized by the exponential growth and dec rates of its (orthogonal) principal axes. These rates, when time-averaged a ordered from the largest, λ_1, to the smallest, λ_N, in an N-dimensional pha space, constitute the "Lyapunov Spectrum" $\{\lambda_i\}$.

An alternative description of this same growth-rate spectrum can based on the time-averaged deformation of infinitesimal 1-, 2-, 3-, dimensional phase-space objects. To generalize the simple property exponential divergence of the one-dimensional distance between neighbori trajectories, it is natural next to consider the divergence (or convergence) infinitesimal two-dimensional phase-space areas, followed by thre dimensional volumes, four-dimensional hypervolumes, and so on. Wh time-averaged, the successive orthogonal growth rates required are again t Lyapunov exponents. The largest, λ_1, describes the rate of divergence of a infinitesimal one-dimensional *length* δr linking two trajectories:

$$\lambda_1 = d\ln\delta r/dt$$

By adding λ_1 to the next largest exponent, λ_2, we get the sum, $\lambda_1 + \lambda_2$ describing the growth rate for a two-dimensional *area* dA defined by thre neighboring trajectories:

$$\lambda_1 + \lambda_2 = d\ln\delta A/dt$$

By adding more dimensions we finally reach the last such relation:

$$\Sigma\lambda_i = d\ln\delta\otimes/dt$$

where the sum includes all N Lyapunov exponents and $\delta\otimes$ is a comovin infinitesimal hypervolume element with the full phase-space dimensionality

Numerical characterization of the complete spectrum of Lyapuno exponents[12] is computationally intensive. What can be done is severel limited by computational speed. In 1989 it is feasible to compute accurat values of hundreds, but not yet thousands, of Lyapunov exponents, an

several such calculations have been carried out. The same basic technique applies for either stationary or time-periodic processes.

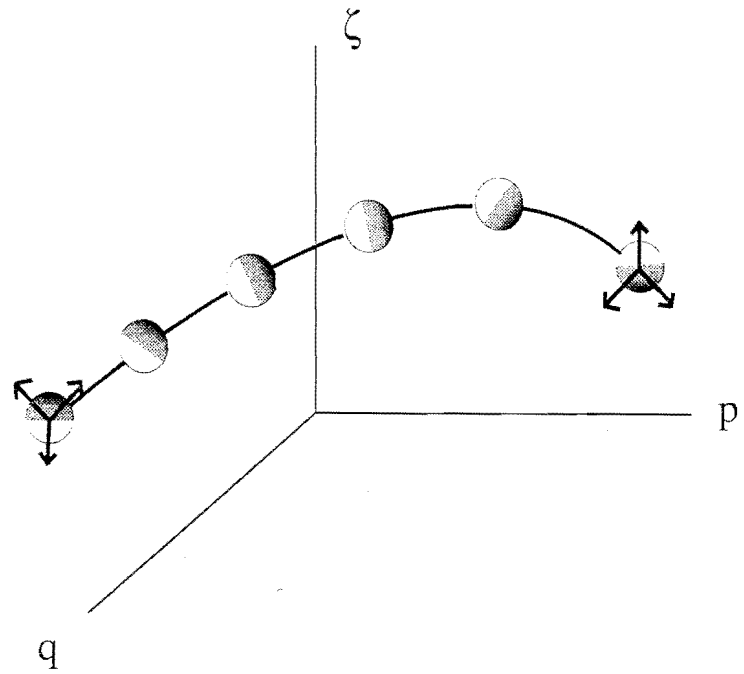

FIGURE 11. The time-development of three comoving and corotating infinitesimal phase-space basis vectors. By measuring the tendency of these vectors to grow, or to shrink, the Lyapunov spectrum can be determined.

Begin by following the construction indicated in Figure 11, erecting a comoving orthonormal set of basis vectors $\{\delta_i\}$, one for each of the N phase-space dimensions, with the origin of the set fixed on an unconstrained moving "reference trajectory". Then the linearized equations of motion of the basis vectors (which can be thought of as describing the motion of N neighboring "satellite trajectories") are solved with the restriction that the basis vectors remain orthonormal. This orthogonality constraint can be repeatedly imposed by Gram-Schmidt orthonormalization. Alternatively, and more elegantly, the constraint can be imposed continuously, by including Lagrange multipliers directly in the equations of motion. In all, N(N+1)/2 multipliers λ_{ij}(or constraints) are required to maintain the orthonormality of N independent basis vectors:

$$d\delta_1/dt = D\cdot\delta_1 - \lambda_{11}\delta_1,$$
$$d\delta_2/dt = D\cdot\delta_2 - \lambda_{22}\delta_2 - \lambda_{21}\delta_1,$$
$$d\delta_3/dt = D\cdot\delta_3 - \lambda_{33}\delta_3 - \lambda_{32}\delta_2 - \lambda_{31}\delta_1,$$
$$\cdots,$$

where the time-averaged values of the diagonal elements $\langle\{\lambda_{ii}\}\rangle$ of the lower triangular array of Lagrange multipliers,

$$\lambda_{ij} = \delta_i\cdot D\cdot\delta_j + \delta_j\cdot D\cdot\delta_i;\ \lambda_{ii} = \delta_i\cdot D\cdot\delta_i$$

are the set of Lyapunov exponents $\{\lambda_i\}$:

$$<\{\lambda_{ii}\}> = \{\lambda_i\}$$

The differential equations determining the Lyapunov exponents through the matrix D turn out to be *odd* in the time so that in the time-reversed motion the most positive Lyapunov exponent becomes the most negative, and *vice versa*. But, because the rotation of the basis vectors $\{\delta\}$ is unconstrained and depends on the past history of the reference trajectory, there is no simple general relationship between the orientations of the vectors going backward and forward in time.

Typical equilibrium Lyapunov spectra[12] for two- and three-dimensional fluids and solids are shown in Figure 12. Such spectra are much less distinctive and informative than the phonon spectra of solid-state physics. Similarly, the spectra of rotation rates of the vectors show little structure, although, unlike the Lyapunov exponents themselves, the rotation rates increase rapidly with system size.

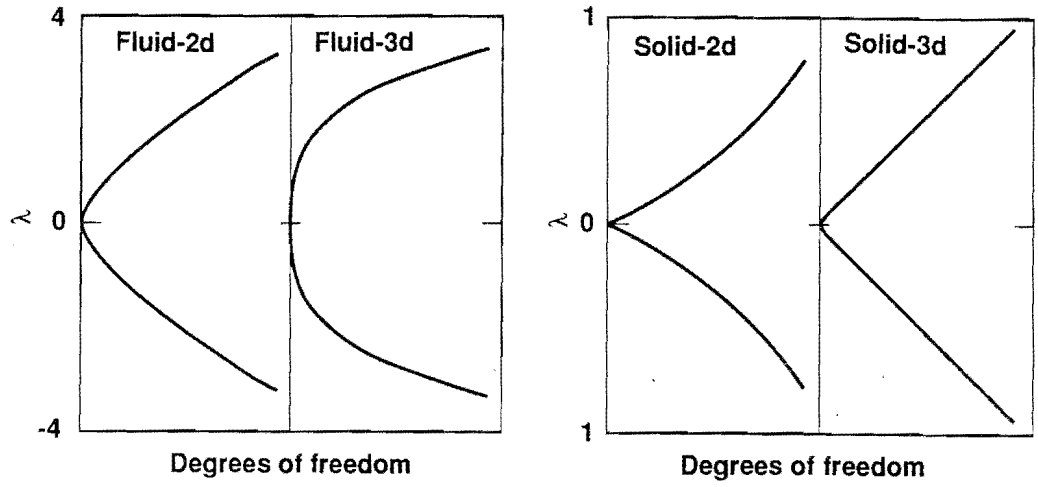

FIGURE 12. Lyapunov spectra for equilibrium two- and three-dimensional fluids and solids. The Lyapunov exponents are arranged in positive-negative pairs, increasing in magnitude from left to right. The number of such pairs is equal to the number of degrees of freedom required to describe the system.

Even *away* from equilibrium the Nosé-Hoover equations for the Lyapunov spectrum are time-reversible. This time symmetry might wrongly suggest that the Lyapunov spectrum remains symmetric about zero. In fact the symmetry is broken because the time-reversed trajectory is even less stable than the original one. Figures 13 and 14 show Lyapunov spectra for two- and three-dimensional boundary-driven steady shear flows. Figure 13 displays spectra for four two-dimensional systems with 4, 9, 16, and 25 Newtonian particles driven by isothermal boundaries. Figure 14 shows two three-dimensional eight-particle systems, one with fixed boundaries, and one with moving boundaries. For all of the five nonequilibrium systems shown in these Figures the Lyapunov exponents are, on the average, negative. Notice that in the equilibrium case shown in Figure 14 the exponents have instead the symmetric distribution suggested by the time symmetry of the equations of motion. This generic nonequilibrium shift away from the symmetric

distribution occurs for any nonequilibrium flow involving the dissipation of concentration, velocity, or temperature differences.

Several interesting conclusions can be drawn from such measured spectra and their nonequilibrium shifts. The negative exponents give directly the rates at which past information is destroyed while the positive exponents give the rate at which future information is created, with the sum of the Lyapunov spectrum corresponding directly to the macroscopic thermodynamic dissipation. It is remarkable that the *dynamic* spectrum is also directly linked to a *static* property of nonequilibrium attractors, the "information dimension", through the Kaplan-Yorke conjecture.

The spectrum is also linked to irreversible thermodynamics. To see this connection let us reexamine the result from Section 2 linking the total change in entropy to the heat transfer associated with Nosé-Hoover thermostats:

$$dS_{TOTAL}/dt = \Sigma -(dQ/dt)/T > 0$$

As before, -DQ represents heat extracted from the nonequilibrium system by its surroundings. Because the frictional forces extract heat at a time-averaged rate equal to the product of the frictional force, $-\zeta p$, and the velocity, (p/m):

$$-\langle dQ/dt\rangle = \langle \zeta p(p/m)\rangle = \langle \zeta\rangle kT$$

the time-averaged heat transfer rates, divided by the corresponding temperatures T, are exactly equal to the friction coefficients ζ for the corresponding thermostatted degrees of freedom. Thus

$$dS_{TOTAL}/dt = k\Sigma\langle\zeta\rangle = k\langle dlnf/dt\rangle > 0$$

Because probability (conserved by *any* flow) corresponds to the product of the probability density f(q,p,t) and the comoving phase-space hypervolume f, the logarithm of the product, $\ln(f\otimes) = \ln f + \ln\otimes$, is constant, and the comoving phase-space hypervolume $\otimes$ must shrink to zero as given by the summed Lyapunov spectrum:

$$kd\ln\otimes/dt = k\Sigma\lambda = -kdlnf/dt = -dS_{TOTAL}/dt$$

Thus there is a direct connection between the rate of thermodynamic dissipation, dS_{TOTAL}/dt, and the Lyapunov spectrum $\{\lambda\}$.

We see that comoving low-dimensional phase-space objects *grow* exponentially in time while high-dimensional objects *shrink*. Kaplan and Yorke made the reasonable conjecture[15] that the time-averaged linearly-interpolated dimensionality of a phase-space object which neither shrinks nor grows, so that $\Sigma\lambda$ vanishes, is equal to the "information dimension" of the corresponding strange attractor. The information dimension can be independently defined by determining, for small phase-space bins of size ε, the dependence of the integrated probability density on the bin size.

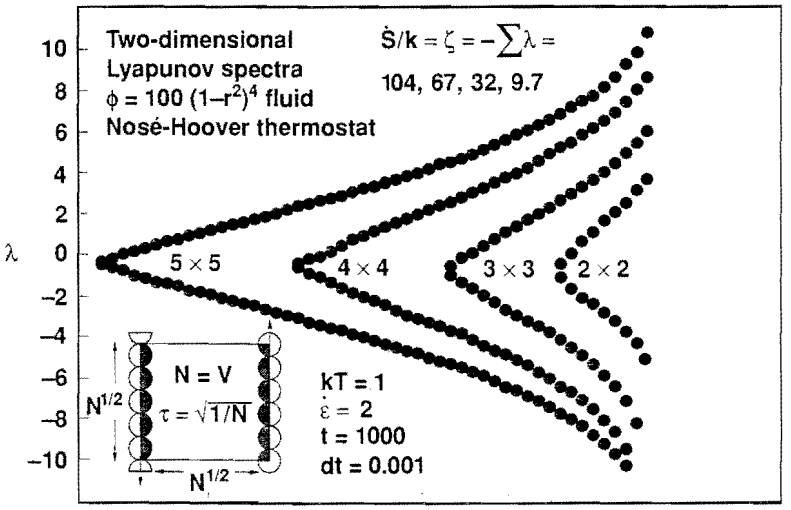

FIGURE 13. Lyapunov spectra for 4-, 9-, 16-, and 25-body two-dimensional boundary-driven steady-state shear flows. Note that the spectra are shifted toward negative values. The sum of the exponents is proportional to the irreversible entropy production.

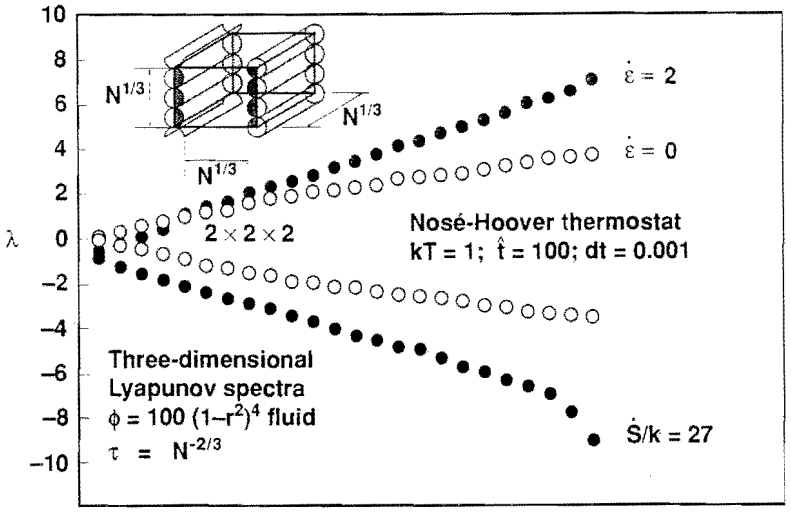

FIGURE 14. Lyapunov spectra for two eight-body three-dimensional systems. The rate-dependence of the spectrum is primarily linear in the strain rate, with an increase in the exponents' magnitudes over those found at zero strain-rate and indicated by open circles (equilibrium). The data also reveal an additional negative shift, approximately quadratic in the strain rate.

In a D-dimensional space an integrated probability density varies as the Dth power of the bin size ε. For singular distributions, in which the probability density approaches zero or infinity as ε vanishes, the variation of bin probabilities with bin size can be determined:

$$P_k(\varepsilon) = N_k(\varepsilon)/N$$

yielding the ratio, $\langle \ln P(\varepsilon) \rangle / \ln \varepsilon$. For small ε this ratio approaches a measure of dimensionality called the "information dimension". The remarkable connection between the dynamic Lyapunov spectrum and the static information dimension has been verified for many simple models. In the following section we explore the concept of fractal dimension in more detail.

4. FRACTALS

A cornerstone of statistical mechanics is the Liouville Theorem result that f(q,p) is unchanged in equilibrium Hamiltonian flows. Then, because f⊗ corresponds to probability, ⊗ must likewise be unchanged by the motion. Away from equilibrium, with heat transfer included, things are different. In nonequilibrium steady states the density f diverges and the volume ⊗ vanishes.

What do the divergence of the stationary probability density f(q,p) and the vanishing of the phase-space volume ⊗ mean? Both singular behaviors seemed mysterious until the steady-state probability density $\langle f(q,p) \rangle$ could be measured and displayed graphically, for relatively-simple systems[14,16-19] with only a few degrees of freedom. The divergence of f signals the formation of a new phase-space object with zero volume but with an intricate and singular probability distribution. The singular phase-space object has structure on two scales. On a *small* scale the distribution approaches infinity exponentially fast, as $e^{-\Delta Q/kT} \propto e^{-\Sigma \lambda t}$, while on a fixed *coarse-grained* scale the integrated probability density slowly converges to a singular structure varying locally as a fractional power of the bin size. These coarse-grained distributions have a "fractal" structure. Apparent holes and gaps appear in the phase space and these cease to vanish or simplify no matter how small the scale of observation. At a sufficiently small scale this structure is no longer physics, but mathematics. In practice the uncertainty principle limits observation scales to roughly 17 digits, so that the scaling relation can exist over no more than 17 orders of magnitude.

Chhabra and Jensen[20] showed how to identify the singularities included in the multifractal structure. This can be done by finding the limiting dependence of moments of the $\{N_k\}$ on the bin size ε. Figure 15 shows the singularity spectrum for a Lorentz gas or "Galton Board" problem detailed in the next section. The spectrum describes the fractal character of two-dimensional "Poincaré-section" cuts through the three-dimensional phase space. The abscissa gives the power-law dependence of the singularity on the bin size and the ordinate the corresponding "bin counting" fractal dimensionality. An ordinary two-dimensional cross section for this problem would correspond to a delta function at the point (2,2). The numerical results show that though most of the distribution corresponds to contraction, with a and f both less than the spatial dimension of two, the nonequilibrium steady-

state distribution also contains anomalous expanding regions, with a probability density that vanishes on a small scale (a > 2).

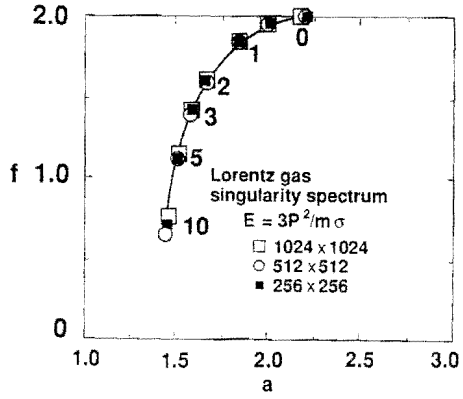

FIGURE 15. The multifractal singularity spectrum for the steady nonequilibrium field-driven Galton Board. The box-counting dimension, f(a), is plotted as a function of the singularity strength a. The singularity strength is the power with which the integrated bin probability depends upon the bin size ε in the small-ε limit.

5. FEW-BODY RESULTS

The study of few-body systems has been useful in understanding the pardoxes associated with irreversibility, thermodynamics, and phase-space structure of nonequilibrium flows. The combination of Runge-Kutta integration with MacIntosh and Stellar Graphics, makes it possible to view results quickly and to preserve them inexpensively on videotape. In this section we describe three such interesting problems: The Galton Board, the Viscous Lorentz Gas, and the Free Expansion in One Dimension.

The Galton Board

For the simplest nonequilibrium steady-state illustration of Nosé-Hoover mechanics consider the Galton Board[14-16] illustrated on the righthand side of Figure 16. The system is a caricature of solid-state diffusion, and involves the field-induced isokinetic (constant-speed) motion of a mass point in a periodic array of scatterers. A parallelogram unit cell is indicated in the Figure. A constant horizontal field tends to drive a moving mass point to the right, parallel to the field direction. The fixed hard-disk scatterers periodically scatter the momentum, with a bias toward head-on collisions. After scattering, the acceleration toward the x direction begins again. A single particle moves through the board, at *fixed* kinetic energy, $p^2/(2m)$, undergoing chaotic mixing collisions with the scatterers. Pas-

reduced to a two-dimensional one, spanned by the two angles (a for position and b for momentum) required to describe a collision. See Figure 17 for a definition of the angles a and b and Figure 16 for the corresponding Poincaré section showing, as separate dots, 10,000 successive collisions.

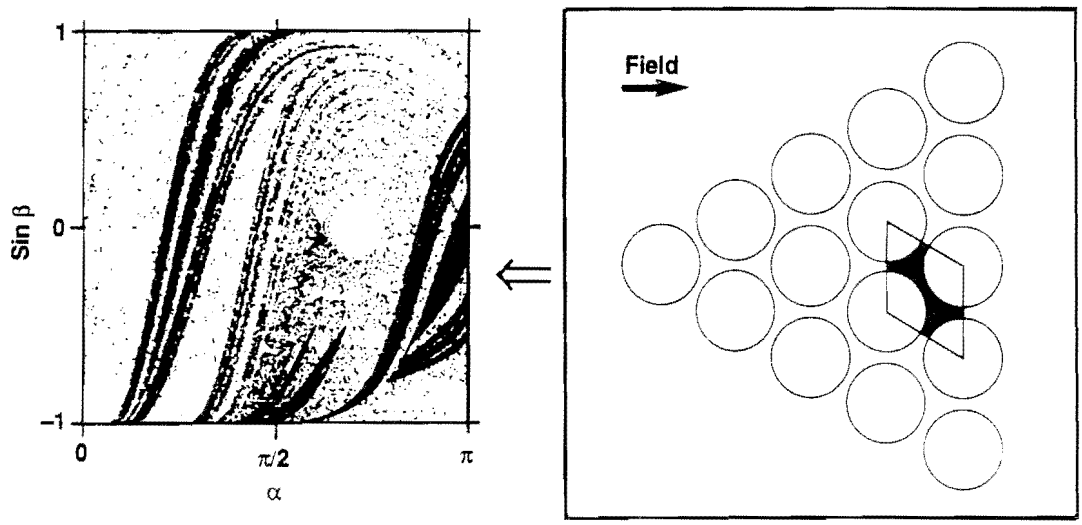

FIGURE 16. The righthand side of the FIGURE indicates the geometry of a finite "Galton Board", in which an external field accelerates a mass point to the right, through the periodic array of scatterers. The values of the two angles, α and β, describing collisions and defined in FIGURE 17, give strange attractors with Poincaré sections of the kind shown on the lefthand side of the FIGURE.

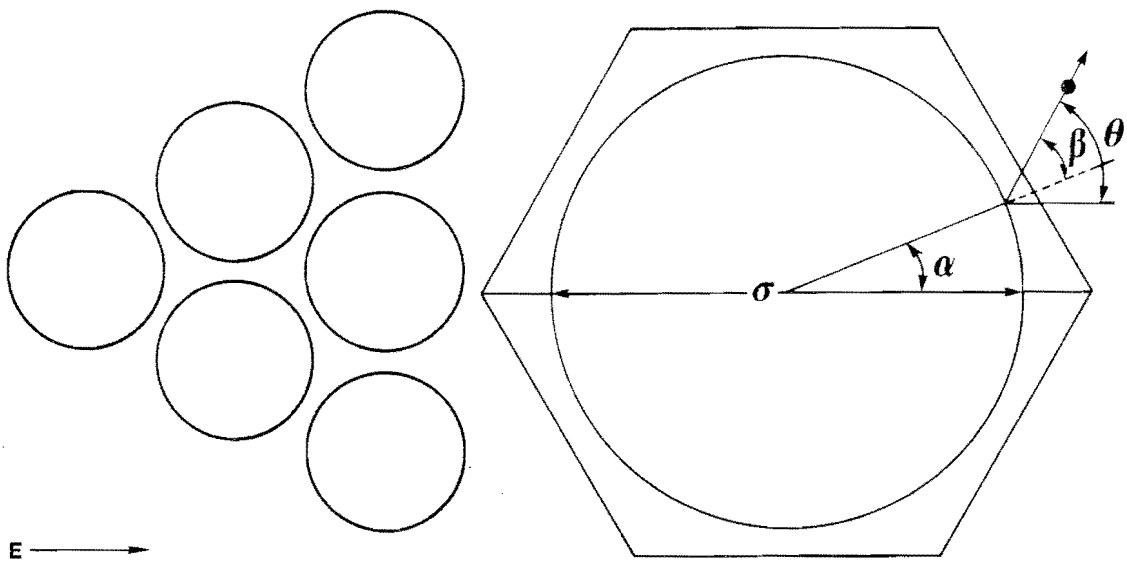

FIGURE 17. Definition of the angles α and β describing Galton-Board collisions.

The equations of motion for the Galton Board problem have simple analytic forms. The basic one, which gives the time variation of the direction of motion between collisions, is

$$d\theta/dt = -pE\sin\theta.$$

A detailed numerical investigation reveals that the resulting flow always behaves irreversibly, as it must, with a positive field-dependent conductivity. The scattering particle moves to lower and lower potential energy at a time-averaged steady rate. The visual appearance of the phase-space distribution converges rapidly to a "strange attractor" with a cross section of the type shown in Figure 16. Visual convergence to a nonequilibrium steady state takes only about 10 collisions. This is shown in Figure 18 by tracing the time history of quadrants of 2500 initial conditions after 1, 2, 3, 5, and 10 collisions each. On a long time scale the intricate multifractal structure penetrates to smaller and smaller length scales.

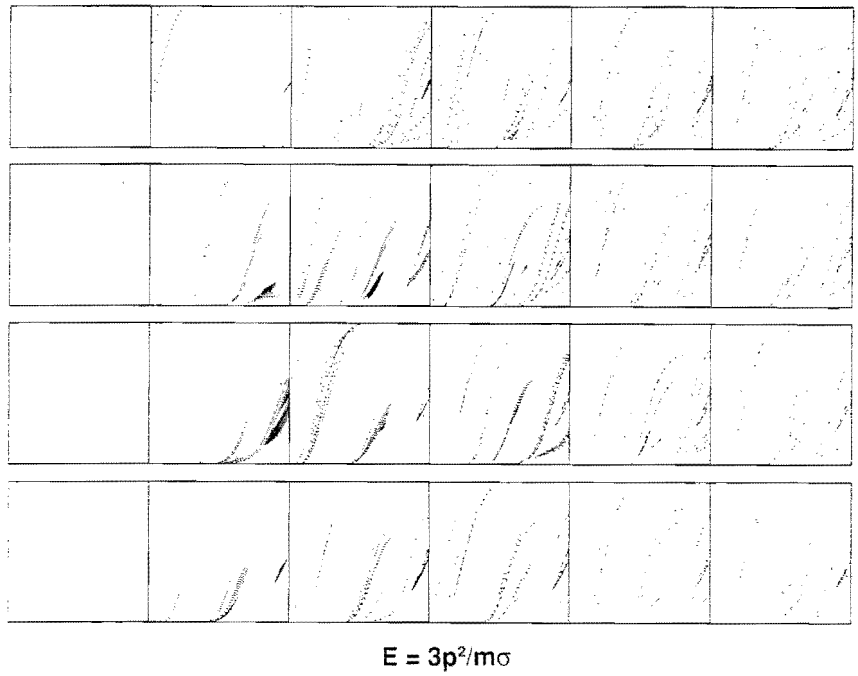

FIGURE 18. Convergence of four sets of 2500 initial conditions, each taking up one-fourth of the phase-space Poincaré section of FIGURE 16, to the steady-state strange attractor. Evolving distributions after 1, 2, 3, 5, and 10 collisions are shown.

The Galton Board fractal objects are fascinating. Successive enlargements show that the structure persists to the smallest feasible scales. See Figure 19 for a series of four enlargements. Such enlargements are used in the logarithmic extrapolation of bin populations to smaller and smaller sizes. The multifractal spectrum of Figure 15 was generated by analyzing a series of enlargements equivalent to ten successive twofold magnifications. At any particular scale numerical work strongly suggests that increasing the number of collisions will eventually fill every bin, no matter how small or improbable. Thus this nonequilibrium steady mixing flow is ergodic, but with the more probable parts of phase-space becoming more and more sparse as the scale of observation is refined. The time-reversibility of the equations of motion implies the existence of a repellor (with the attractor velocities reversed--see Figure 20). It is an amazing consequence of the ergodic nature of the flow that every repellor point lies arbitarily close to attractor points, and *vice versa*. The plausibility of this ergodicity is apparent from the more-

detailed Figure 21, which shows 640,000 points distributed over a computer-generated print originally covering an area of one square meter.

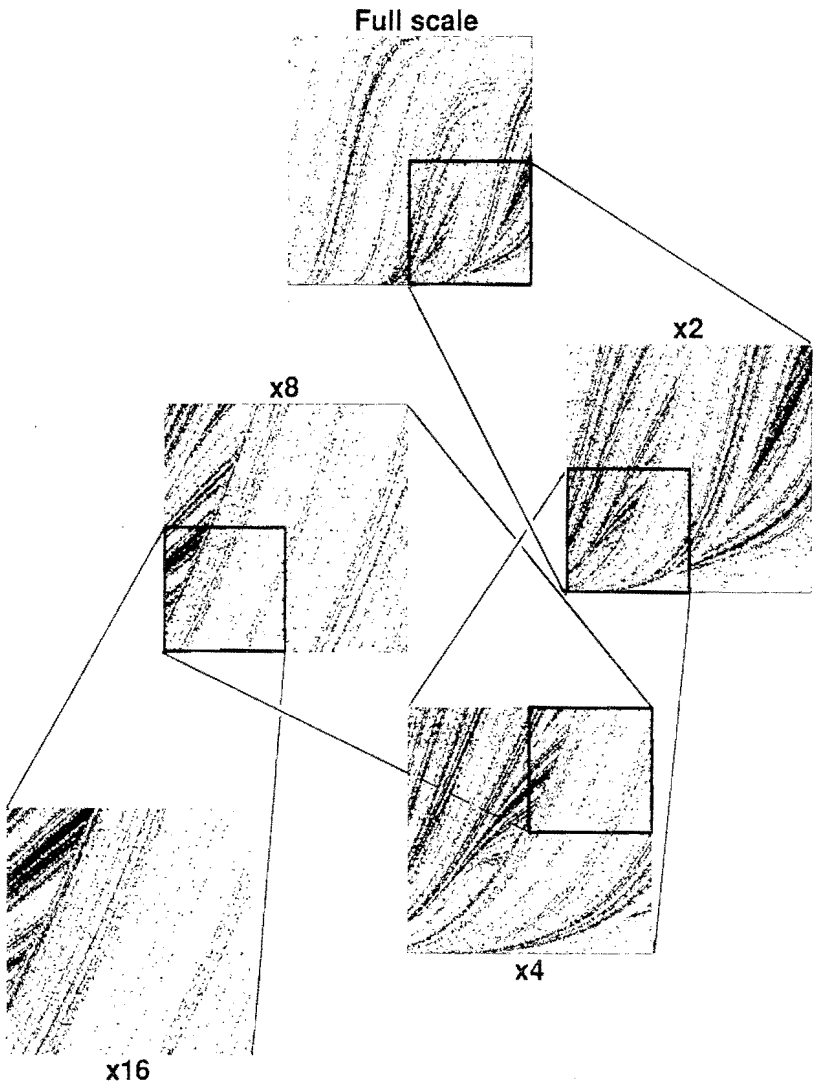

FIGURE 19. Galton Board attractor structure shown at 2-, 4-, 8-, and 16-fold magnification. In each snapshot 10,000 collisions are shown.

The Galton Board motion takes place in a three-dimensional phase space and accordingly has three Lyapunov exponents. One is positive, giving the mean rate of growth in phase-space separation due to scattering off the convex surfaces. One is zero, corresponding to the motion along the trajectory direction. One is negative, sufficiently so that the three-term exponent sum is negative and equal to the rate of total entropy increase $dS_{TOTAL}/dt = -(dQ/dt)/T$. For certain ranges of field strength the positive Lyapunov exponent changes sign and the motion collapses onto a one-dimensional limit cycle with a Poincaré cross section composed of a few discrete dots.

This Galton Board problem provides a nice mechanical illustration of the Second Law of Thermodynamics. The requirement that the phase-space distribution is confined to a finite region of space implies that the time-averaged friction coefficient ζ be positive and that the particle therefore moves from higher to lower potential energy. If the friction were negative the energy

would eventually diverge. If the friction were zero there could be no average current.

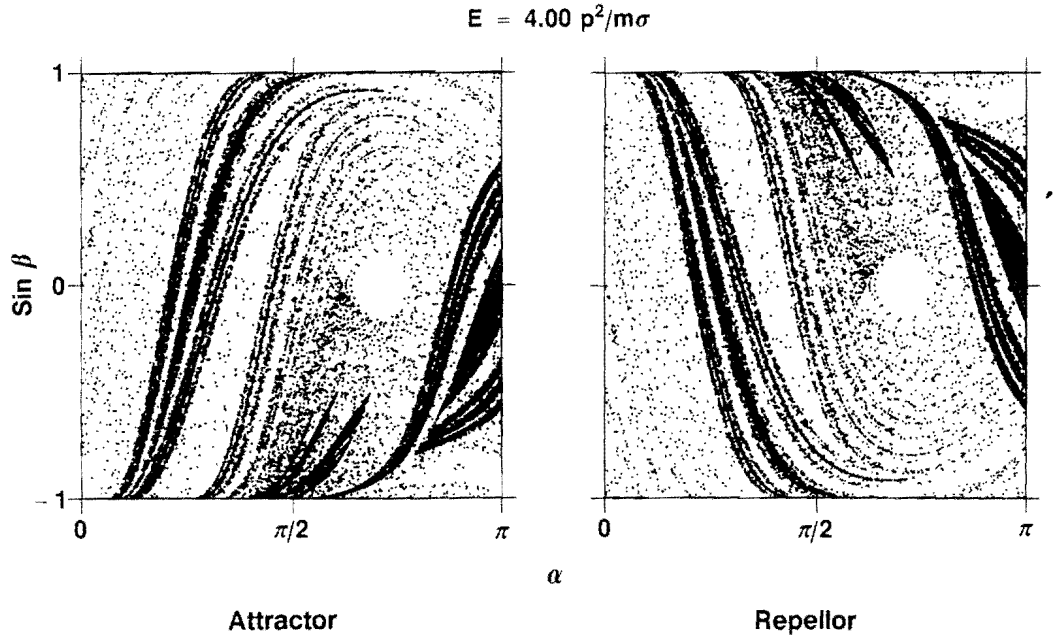

FIGURE 20. Galton Board attractor and repellor sections. Because the equations of motion are time-reversible the reversed (repellor) motion corresponds to a reflection of the attractor about a horizontal line. This changes the sign of the velocity angle β.

Series of related many-body simulations, with half the particles accelerated in one direction by a field and the rest in the opposite direction, gave analogous results. The dimensionality of the many-body strange attractor describing the motion varied quadratically with the field strength (as would be expected from the mirror symmetry linking positive field and negative field results).

The Viscous Lorentz Gas

Numerical analysis of a time-varying problem is complicated by the additional phase-space dimension. Time variation can be introduced through a varying external field or by using time-periodic boundary conditions. A periodic shear (See Figure 22 for a three-dimensional version) is the simplest example, and the two-body "Lorentz Gas" shear flow is the simplest of these. The viscous Lorentz Gas[18] resembles the Galton Board. The viscous flow can be thought of as a symmetric two-body problem, or as an equivalent one-body scattering problem, but now with the boundaries moving at a rate given by the macroscopic constant strain rate. Four unit cells of such a periodically-shearing system are shown, at five equally-spaced times, in Figure 23.

The local motion of a moving particle, relative to the systematic velocity u_x, can be constrained to be isokinetic, by using Gauss' Principle of Least Constraint. If this is done, the resulting equation of motion, *between* collisions, is again simple,

$$d\theta/dt = \gamma \sin^2\theta$$

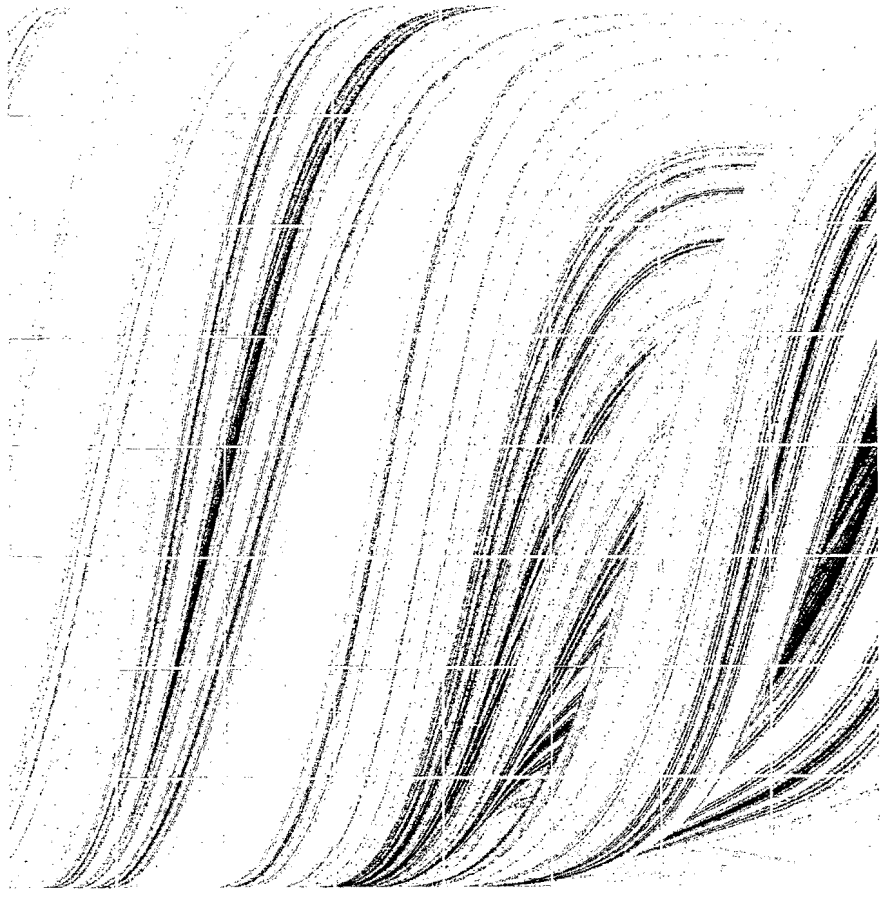

FIGURE 21. Details of the full attractor Poincaré section of FIGURE 19 representing 640,000 successive collisions. The original computer-generated picture was one square meter in size. Numerical analyses using 1000 times as many points as are shown here are currently feasible.

where γ is the "strain rate",

$$\gamma = du_x/dy$$

The hard-disk scattering analysis can be simplified by considering the large-F limit of a *constant* repulsive central force F. With this assumption the equation of motion *during* collisions,

$$d\theta/dt = (F/p)\sin(\alpha-\theta)$$

can likewise be integrated analytically. By taking the large-F limit and using a geometric condition, that the polar-coordinate integral of dr/dt *through* a collision vanishes, the post-collision direction of motion can be found as the solution of a single transcendental equation. In the large-F limit the angle α, which measures the location of the scattering particle relative to the x axis, is constant during a collision.

This problem is periodic in time, as well as in space, because in a time equal to $1/\gamma$ the system progresses from one checkerboard-like configuration to the next. For an initially-square unit cell, a shear of unity, corresponding to an oblique-cell corner angle of 45°, brings the system back to its original configuration. See again Figure 23 for a four-cell square-corner version of

this periodic shear flow. Thus, in addition to the two angles describing a collision, the *phase* of the boundary condition must be specified, making the Poincaré-section description of successive collisions a three-dimensional problem. Nevertheless, a bin structure of 2,097,152 = 2^7x2^7x2^7 bins is sufficient to determine an accurate multifractal spectrum of singularity strengths. The results are similar to those shown for the Galton Board in Figure 15. We find no trace of the cusps found by Morriss in his analysis of a similar soft-disk problem[19].

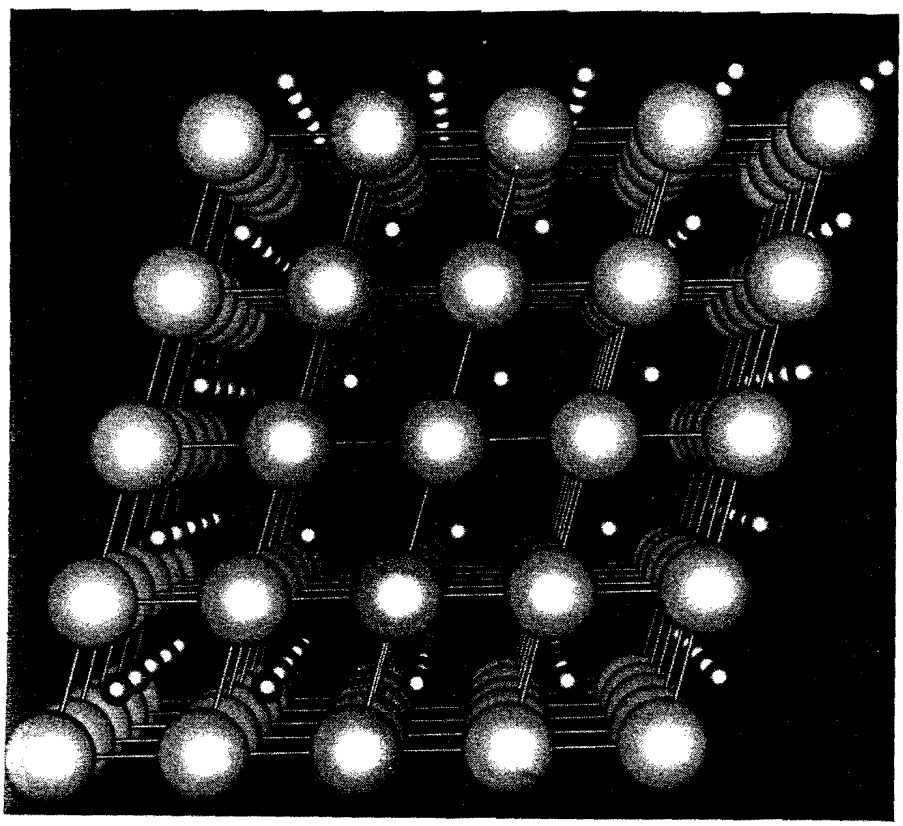

FIGURE 22. A two-body three-dimensional periodic shear flow. For convenience in identifying the unit cell (125 cells are shown in the FIGURE) the two particles are shown as spheres with different diameters.

The distribution of Poincaré-section points in the four-dimensional Lorentz-gas' phase-space, corresponding to the information dimension D_1, is shown in a pair of stereo views in Figure 24. To see this "Poincaré cube" in three dimensions make a copy of this Figure in which the spacing between the centers of the left-eye and right-eye images corresponds to the distance between your own eyes. A viewing distance of about 30 cm is best.

The two angles describing the collisions, α and β, are displayed as a function of the shear (the axis perpendicular to the plane of the paper). This shear-flow problem has a somewhat simpler appearing Poincaré-cube structure than does the diffusive Galton Board problem, despite the extra phase-space dimension. Just as in the Galton Board case the Poincaré cube pictures suggest the filling of all bins with a zero-volume completely-ergodic chaotic attractor.

At sufficiently high strain rates the motion collapses onto a one-dimensional periodic limit cycle. In the resulting Poincaré-cube representation such a cycle appears as a discrete set of dots. In either of these steady nonequilibrium two-body problems, diffusion or shear, the strange-attractor motion develops so as to give positive transport coefficients consistent with the Second Law of Thermodynamics.

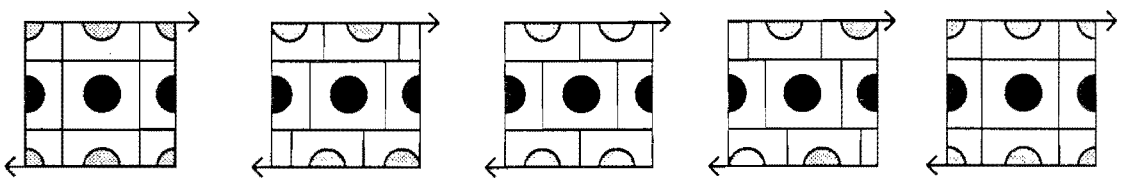

FIGURE 23. Moving boundary particles for the two-dimensional periodic two-body viscous Lorentz gas discussed in Section 5. The square shown represents an area of four unit cells. Only the periodically-repeated Boundary particle is shown. A mass point moves in the field of these particles. Snapshots corresponding to shears of 0, 1/4, 2/4, 3/4, and 1 (equivalent again to 0) are shown.

Free Expansion in One Dimension

There are many paradoxes associated with the thermodynamics of incompressible phase-space flow described by Liouville's Theorem. The best known is an adiabatic free expansion in which the expanding fluid does no external work, accepts no heat, and hence expands at constant energy. The paradox is that the phase-space density, which, according to Gibbs, should vary with entropy, remains unchanged in the process while the thermodynamic entropy increases. This paradox can be resolved, or at least avoided, by using Nosé-Hoover mechanics to embed the paradoxical expansion in a periodic process. This approach emphasizes the importance of interactions with external forces in any process designed to measure entropy. To embed the free expansion in a periodic process consider a three-step periodic cycle:

i) Expand the volume instantaneously.
ii) Compress the system, at a finite rate, back to the initial volume.
iii) Thermostat the dense hot system to restore the original temperature.

The simplest realization of this cycle is one-dimensional. To represent a system initially confined we consider a thermostatted particle in a simple one-dimensional "box" given by a harmonic Hooke's-Law potential:

$$\phi = x^2/2$$

To start a periodic expansion, compression, and thermalization cycle the potential ϕ changes discontinuously to the new form:

$$\phi = \{(x+1)^2/2 \quad \text{or} \quad 0 \quad \text{for} \quad -1 < x < 1 \quad \text{or} \quad (x-1)^2/2\}$$

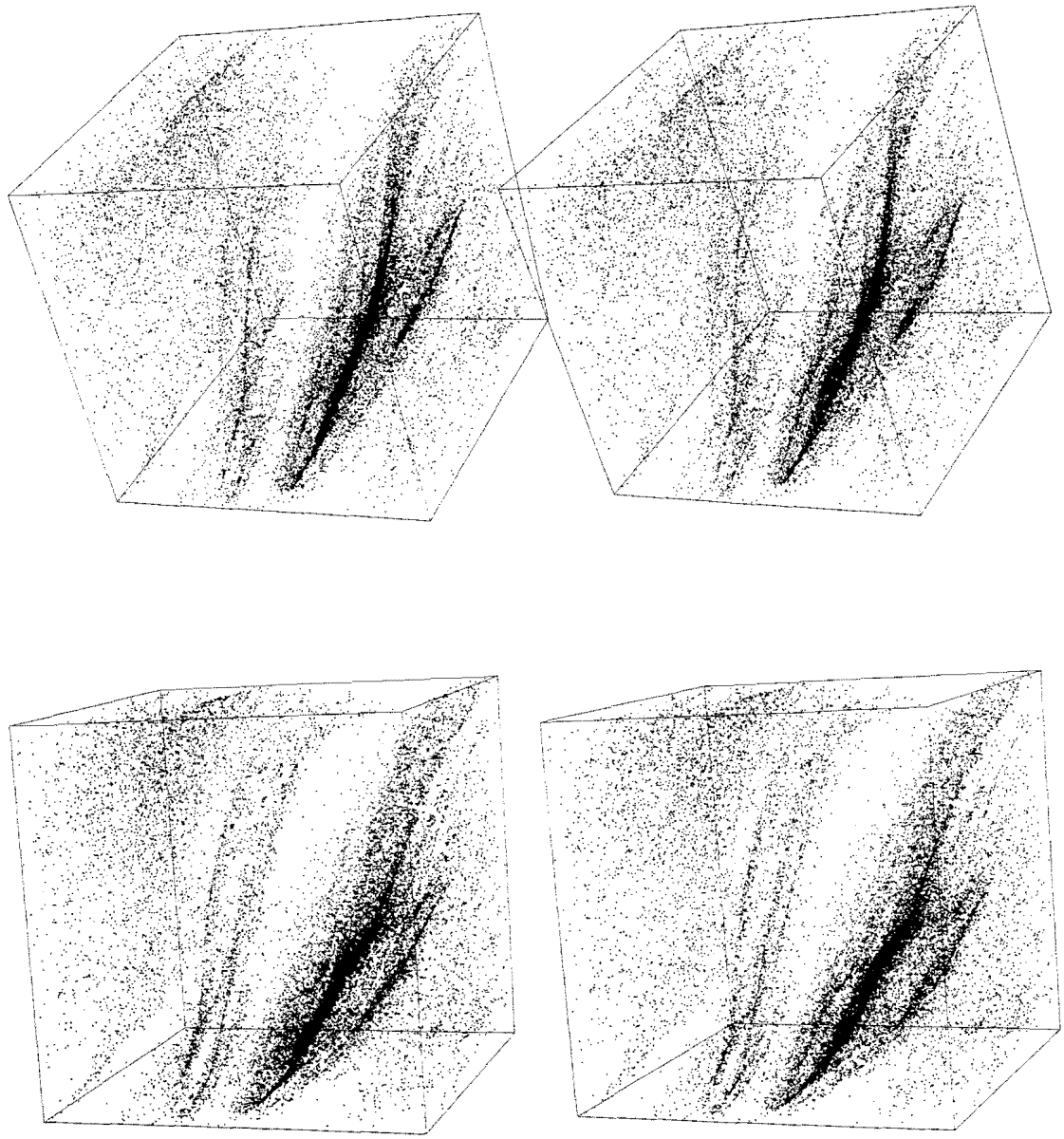

FIGURE 24. Two stereo views of the phase-space Poincaré cube detailing the phase-space distribution of collisions for the two-dimensional shear flow of a Lorentz Gas driven by the periodic boundaries of FIGURE 23. The (mainly) vertical and horizontal axes correspond respectively to $\sin\beta$ and α. The axis (mainly) perpendicular to the plane of the paper represents strain, or equivalently, phase, in the time-periodic boundary motion of FIGURE 23.

Next, over a relatively long period of 1000 fourth-order Runge-Kutta time steps of length dt = 0.01 each, the moving particle is slowly and steadily compressed. This adiabatic compression, at one tenth the thermal velocity, corresponds thermodynamically to a nearly-isentropic process. Finally, the compressed particle is thermostatted, using Nosé-Hoover mechanics, by solving the equations of motion

$$dx/dt = p \qquad dp/dt = - x - \zeta p \qquad d\zeta/dt = (p^2 - 1)/\tau^2$$

where the relaxation time, τ, is 0.1. The thermostatting is applied over the shortest interval such that ζ begins and ends at zero. The particle mass has been chosen equal to one, for convenience.

This three-step irreversible thermodynamic process, incorporating expansion, compression, and thermalization, is perfectly time-reversible, obeying the same equations of motion in either direction of time. Nevertheless the requirement that the occupied phase space not diverge implies that the motion can only converge to a zero-volume strange attractor. By Liouville's Theorem, the phase volume is unchanged during both the expansion and compression steps. Thus the thermalization must, on the average, contract the occupied phase volume.

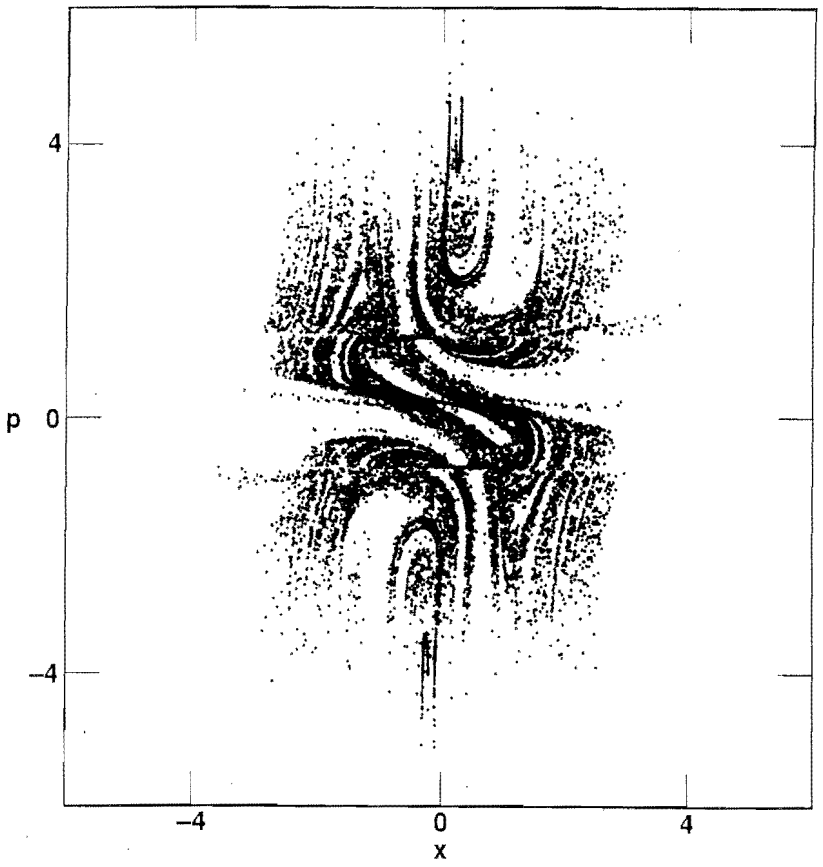

FIGURE 25. Strange attractor Poincaré section corresponding to the one-dimensional free expansion described in the text. After the expansion, compression, and thermalization stages, at the instant just preceding the next expansion, the momentum is plotted as a function of the particle coordinate. The Lyapunov-unstable strange attractor reflects the entropy increase associated with free expansion.

Numerical work confirms this conclusion. Figure 25 shows a Poincaré section of the resulting strange attractor. Just as in the Galton Board and Viscous Lorentz Gas the fractal structure is apparent. It can be verified that the dissipation associated with the thermostatting exactly accounts for the irreversible entropy production associated with the free expansion step. Thus the Nosé-Hoover mechanics makes it possible to analyze transient irreversibility too, by embedding the problem in question in a periodic process.

6. SUMMARY

To describe irreversible processes at an atomistic level it is convenient to apply boundary constraints using Nosé-Hoover mechanics. The inevitable conversion of work to heat, summarized by the Second Law of Thermodynamics, appears in *any* nonequilibrium state, steady, periodic, or transient. With Nosé-Hoover reversible and deterministic mechanics, the direction of the motion is determined by the geometric requirement that the phase-space volume cannot grow with time. By using techniques borrowed from nonlinear dynamics it can be established that the resulting phase-space structures are strange attractors, hosts of chaotic, microscopically reversible but macroscopically irreversible motion. The magnitude of the shrinking within the attractor depends only on the work done by external forces, or, equivalently, the heat extracted by Nosé thermostats. The information dimension of the motion in phase space can be estimated from the Lyapunov spectrum and more highly correlated fractal dimensions can be obtained by bin-counting methods. The complexity of chaotic many-body flows will ultimately be understood through study of few-body caricatures of the type described here.

ACKNOWLEDGMENT

It is a pleasure to acknowledge the continuing counsel and inspiration of Harald Posch and Brad Holian. We thank Kirk T. Hadley and Paul H. Dunlap for painstaking artistic assistance.

REFERENCES

* This work was supported by the Department of Energy and performed at the Lawrence Livermore National Laboratory under the auspices of the University of California pursuant to Contract W-7405-Eng-48.

1. J. Gleick, **Chaos, Making a New Science** (Viking, New York, 1987).
2. J. A. Yorke, "**Chaotic Dynamics**" (NASA Ames, California Lectures of 12 July 1989, unpublished).
3. See the Proceedings of Recent Meetings of the Materials Research Society (November 1988, Boston, for instance) and topical conferences of the American Physical Society such as **Shockwaves in Condensed Matter 1987**, S. C. Schmidt and N. C. Holmes, Eds. (North-Holland, Amsterdam, 1988)
4. E. Meiburg, Phys. Fluids 29, 3107 (1986).
5. M. Mareschal, M. M. Mansour, A. Puhl, and E. Kestemont, Phys. Rev. Letts. **61**, 2550 (1988).
6. E. N. Lorenz, J. Atmos. Sci. **20**, 130 (1963).

7. F. F. Abraham, W. E. Rudge, D. J. Auerbach, and S. W. Koch, Phys. Rev. Letts. **52**, 445 (1984).
8. A. J. DeGroot, S. R. Parker, and E. M. Johansson, **SVD and Signal Processing, Algorithms, Applications, and Architectures** (North-Holland, Amsterdam, 1988)
9. S. Nosé, Mol. Phys. **52**, 255 (1984) and **57**, 187 (1986); and J. Chem. Phys. **81**, 511 (1984). W. G. Hoover, Phys. Rev. **A31**, 1695 (1985).
10. J. Jellinek and R. S. Berry, Phys. Rev. **A38**, 3609 (1988).
11. B. L. Holian, W. G. Hoover, and H. A. Posch, Phys. Rev. Letts. **59**, 10 (1987); W. G. Hoover, Phys. Rev. A37, 252 (1988).
12. H. A. Posch and W. G. Hoover, Phys. Rev. A39, 2175 (1989).
13. W. G. Hoover, **Lecture Notes in Physics #258: Molecular Dynamics** (Springer-Verlag, Heidelberg, 1986).
14. W. G. Hoover and B. Moran, Phys. Rev. **A** (in press, 1989).
15. H. G. Schuster, **Deterministic Chaos** (Physik-Verlag, Weinheim, FRG, 1984).
16. W. G. Hoover, C. G. Tull, and H. A. Posch, Phys. Lett. **A131**, 211 (1988).
17. W. G. Hoover, H. A. Posch, B. L. Holian, M. J. Gillan, M. Mareschal, and C. Massobrio, Mol. Sim. **1**, 79 (1987).
18. B. Moran, W. G. Hoover, and S. Bestiale, J. Stat. Phys. **48**, 709 (1987).
19. G. P. Morriss, Phys. Rev. **A39**, 4811 (1989); G. P. Morriss, Phys. Lett. **122A**, 236(1987); A. J. C. Ladd and W. G. Hoover, J. Stat. Phys. **38**, 973 (1985).
20. A. Chhabra and R. V. Jensen, Phys. Rev. Letts. **62**, 1327 (1989).